Calibration report for ZephIR Dual Mode lidar (unit 351)

Borraccino, Antoine; Courtney, Michael

Publication date:
2016

Document Version
Publisher's PDF, also known as Version of record

UniTTe

Innovation Fund Denmark
RESEARCH, TECHNOLOGY & GROWTH

DTU

Calibration report for ZephIR Dual Mode lidar (unit 351)

DTU Wind Energy E-Report-0088

A. Borraccino[1], M. Courtney[1]

DTU Wind Energy E-0088

March 2016

DTU Wind Energy
Department of Wind Energy

Author(s): A. Borraccino[1], M. Courtney[1]

Title: Calibration report for ZephIR Dual Mode lidar (unit 351)

Department: DTU Wind Energy[1]

Abstract:
Nacelle-based profiling LiDARs may be the future of power performance assessment. Due to their large rotor size, single-point measurements are insufficient to quantify the power modern wind turbines can harness. The available energy in the wind indeed varies with heights. Improving power performance assessment by measuring simultaneously at different heights has been demonstrated using ground-based profiling LIDARs. Using nacelle lidars avoids the erection of expensive meteorology masts, especially offshore.

As for any other measuring system, lidars measurements have uncertainties. Their estimation is the ultimate goal of a calibration: a relation is established between reference measurements from calibrated instruments and corresponding LiDAR indications. Traceability in the calibration is obtained by transferring measurement uncertainties from the reference instrument through the calibration process.

A generic methodology to calibrate profiling nacelle lidars has been developed and performed on a ZephIR Dual Mode lidar manufactured by *ZephIR LiDAR*. In essence, the generic methodology calibrates the inputs of the wind reconstruction algorithms rather than their outputs.

This report presents the calibration procedures and results of the ZephIR Dual Mode lidar unit 351. The calibration was performed at DTU's test site for large wind turbines, Høvsøre, Denmark. The methods to assess line-of-sight velocity uncertainties are detailed together with an example of how to derive reconstructed wind parameters' uncertainties.

DTU Wind Energy E-0088

March 2016

ISBN: 978-87-93278-38-7

Contract no.: Innovationsfondens 1305-00024B

Project: UniTTe
http://www.unitte.dk/

Funding:
Innovation Fund Denmark

Pages: 70
Tables: 26
Figures: 10
References: 9

Technical University of Denmark
DTU Wind Energy
Risø Campus
Frederiksborgvej 399
DK-4000 Roskilde
Denmark

www.vindenergi.dtu.dk

Table of contents

Figures and tables

Nomenclature

a.g.l.: above ground level
CW: continuous wave
DK: Denmark
GPS: global positioning system
GUM: Guide to the expression of uncertainty in measurement [6]
HWS: horizontal wind speed
IEC: the International Electrotechnical Commission
LiDAR: light detection and Ranging
LOS: line-of-sight
R&D: Research and Development
RSS: residual sum of squares
RWS: radial wind speed
SI: International System of unis
SQL: Structured Query Language
SSR: sum of squares of residuals
VIM: International vocabulary of metrology [5]
WD: wind direction
ZDM: ZephIR Dual-Mode

α: cone or half-opening angle
α_{th}: theoretical value of cone angle
α_m: measured value of cone angle
α_{exp}: shear exponent of the assumed wind profile
β: effective half-opening angle
β_h: effective horizontal half-opening angle
β_v: effective vertical half-opening angle
ΔH_{pos}: height difference between lidar beam and reference instrument
ΔRWS: radial wind speed measurement error
θ: wind direction
θ_0: estimation of $\mathrm{LOS_{dir}}$
θ_{proj}: projection angle used to evaluate LOS_{dir}
φ_{BE}: best estimate of lidar tilt angle
$\varphi_{indicated}$: lidar indicated tilt angle
φ_{flow}: flow tilt angle
φ_{meas}: measured reference tilt angle
$\varphi_{physical}$: lidar's beam physical inclination
ψ_{BE}: best estimate of lidar roll angle
$\psi_{indicated}$: lidar indicated roll angle
ψ_{ref}: best estimate of lidar roll angle
$\langle\ \rangle$: scalar time average
$\langle\ \rangle_{\mathrm{vec}}$: vector time average
cov: covariance
$r(x, y)$: cross-correlation coefficient between x and y
$stdv$: standard deviation
σ_X: standard deviation of X

D_{cal}: calibration range
$D_{physical}$: total distance between lidar and mast
f_{fit}: fitting function
H_0: height difference between the reference lidar's point and the detected central beam position
H_{mast}: height of meteorology mast a.g.l.
H_{lidar}: height of lidar a.g.l.
k: coverage factor
LOS_{dir}: LOS direction
(N_X, E_X, Z_X): 3D coordinates of X as measured with a total station
R_{fit}: fitted radius of ZDM circular scanning pattern
$Ref_{eq\ RWS}$: reference equivalent radial wind speed
R_{ij}: cross-correlation tensor between uncertainty components
RWS_{norm}: normalised radial wind speed
RWS_{BE}: best estimate of radial wind speed
$RWS_{indicated}$: lidar indicated radial wind speed
S_{hub}: lidar estimated horizontal wind speed at hub height
u_X: standard uncertainty of X
$u_{c,X}$: combined standard uncertainty of X
U_X: expanded uncertainty of X
u_φ: physical tilt inclination angle uncertainty
u_{cal}: calibration uncertainty of cup anemometer HWS
$U_{ext,X}$: extrapolated expanded uncertainty for LOS X
u_H: height uncertainty
u_{inc}: inclined beam uncertainty
$u_{LOS\ dir}$: LOS direction uncertainty
u_{mast}: mounting uncertainty of reference instrument on mast
u_{ope}: operational uncertainty of cup anemometer HWS
u_{pos}: positioning uncertainty
u_{range}: lidar measurement range uncertainty
u_{WD}: wind direction uncertainty
U: streamwise component of the horizontal wind speed vector
V: spanwise component of the horizontal wind speed vector
V_{rX}: radial or line-of-sight velocity of beam X

Preface

This document is the calibration report of the ZephIR Dual Mode lidar – unit number 351. It has been written within work package 2 of the Unified Turbine Testing project (UniTTe, http://www.unitte.dk/) funded by *Innovation Fund Denmark*. UniTTe aims at developing power performance testing procedures using profiling nacelle-mounted lidars applicable in all types of terrain. Work package 2 focuses specifically on developing and performing calibration procedures to provide traceable lidars' measurements once installed on a turbine's nacelle.

One of the two lidars tested in UniTTe is a conically scanning continuous wave system developed by *ZephIR lidar*. Its calibration was performed at DTU Wind Energy's test site for large wind turbines, Høvsøre, Denmark. The calibration procedures have been implemented following the *"Generic methodology for calibrating nacelle lidars"* described in deliverable D2.1 (DTU E-0086 report).

The calibration report is deliverable D2.3 and provides testing details specific to the ZephIR Dual Mode lidar together with the calibration results and measurement uncertainties.

Antoine Borraccino
Ph.d.-student

Acknowledgements

I would first like to thank M. Courtney and R. Wagner who guided the work performed and reported in this document. This report really builds on M. Courtney's pioneering work on lidars' calibration and on the experience of the whole TEM section at DTU Wind Energy in calibrating ground-based, nacelle-based or even scanning lidars.

Thanks to M. Harris, C. Slinger and ZephIR lidar for supporting the UniTTE project and giving the opportunity to test the ZephIR Dual-Mode lidar. Thanks to S.A. Sørensen (DTU-TEM's database engineer) for answering all my database requests. Finally, a special thank you to DTU Wind Energy technicians P. Hansen, A. Ramsing Vestergaard, L. Christensen and K. Schrøder for imagining, designing and building all the necessary testing tools and for their expertise in lidars' beam detection.

Chapter 1

1 Introduction

1.1 Profiling nacelle lidars in power performance testing

In the recent years, the rapid increase in wind turbines size has created a need for developing new power performance assessment procedures. The effects of wind speed and direction variations over the rotor swept area on power curves can no longer be neglected [1]. Measuring the wind in one point, e.g. hub height, has consequently become insufficient.

LIght Detection And Ranging (lidar) is a remote sensing technology addressing this challenge. Its multiple applications have found their way into the wind energy market. Ground-based lidars are presently being used to measure wind profiles. They offer a practical and accurate solution for measuring wind over the entire rotor disk. On the other hand, even though two-beam nacelle lidars are unable to measure the wind shear, they show promising capabilities to assess power performance [2].

A wind profiling nacelle lidar measures the wind at multiple heights upstream of a turbine and from its nacelle – or downstream for wake measurements – thus eradicating the need for expensive meteorology masts, especially offshore. Additionally, nacelle lidars follow the turbine's movements. Consequently, in flat terrain or offshore, the exclusion of wind direction sectors for power performance analysis is limited to wakes from neighbouring turbines and is not required as often as with ground-based or floating lidars.

1.2 The ZephIR Dual Mode lidar

1.2.1 Presentation

The ZephIR Dual Mode lidar (ZDM, see Figure 1) has been developed by *ZephIR Lidar*. This profiling nacelle lidar is a commercially available product. The "dual mode" capability refers to its suitability for both turbine-mounted and ground-based lidar applications. In the UniTTe project, the focus is entirely on the turbine-mounted application.

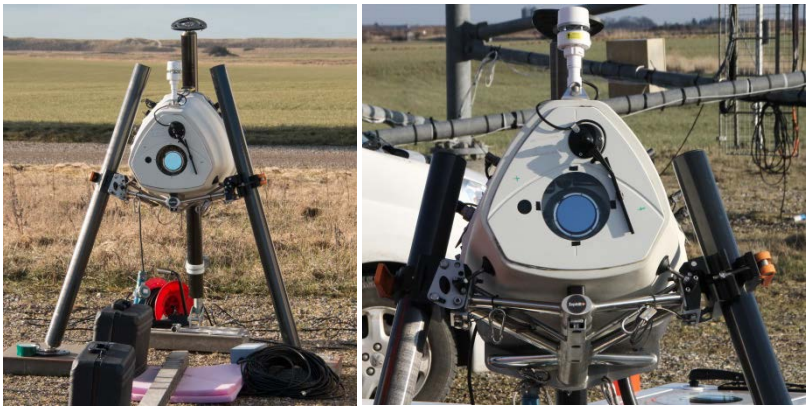

Figure 1. The ZDM lidar (unit 351) during its calibration in Høvsøre, DK

1.2.2 Geometry and main measurement specifications

The ZDM lidar is a homodyne continuous wave (CW) Doppler system. It is an upgrade of the ground-based Z300 lidar allowing to place it horizontally on the nacelle of a turbine. ZDM uses the rotation of a prism to measure in a fixed conical scanning pattern (Figure 2). The cone angle is thus constant: $\alpha_{th} = 14.97°$ (manufacturer specification).

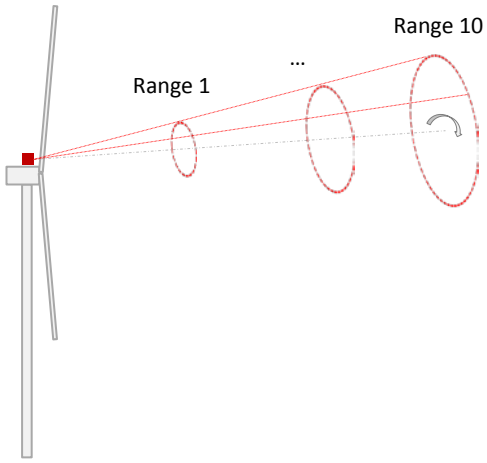

Figure 2. Schematic of the ZDM lidar (ZephIR) mounted on the nacelle of a wind turbine

At any specific range, the scanning pattern is circular. Each revolution takes one second and, on average, 48.8 azimuth sectors[1] are measured (see Figure 3). One Line-Of-Sight (LOS) velocity is obtained by averaging ~4000 Doppler spectra over an azimuth sector of $360/48.8 \approx 7.38°$. Because the number of sectors is not an integer, the central azimuth of one sector will change slightly from one revolution to the next.

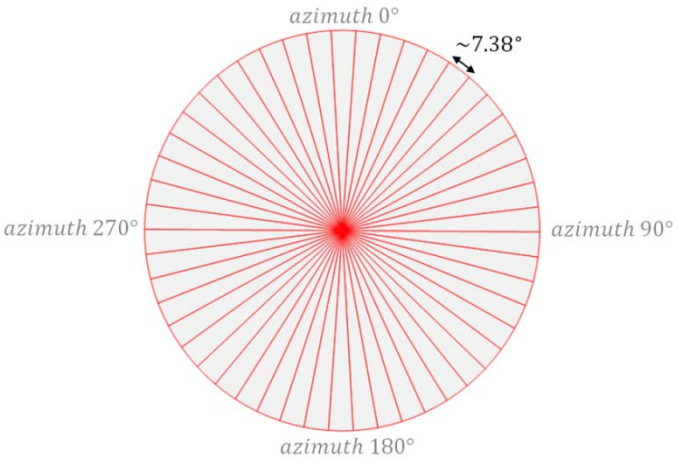

Figure 3. Scanning geometry of the ZDM lidar: ~50 LOS / revolution

User-selected ranges are measured successively by re-focusing the laser beam. ZDM is able to measure at ranges between $10 - 300m$, and a maximum of 10 ranges can be configured. However, being a CW lidar, the probe length increases with the range ($\propto Range^2$) from $\sim 10cm$ at $10m$ to $\sim 60m$ at the range of $300m$. Figure 4 shows the probe length value as a function of the measurement range set in the lidar software. The probe length is calculated as the Rayleigh range of a Gaussian beam at the HWHM (Half-Width at Half-Max) point of the Lorentzian sensitivity function.

[1] The detector output is sampled at 100 MHz by the ADC converter. The FFT is performed in 512 successive time domain scans, providing 2*256 frequency bins. And, 4000 spectra are averaged. Thus the resulting measurement frequency is: $100\ MHz/(512 * 4000) \approx 48.8\ Hz$.

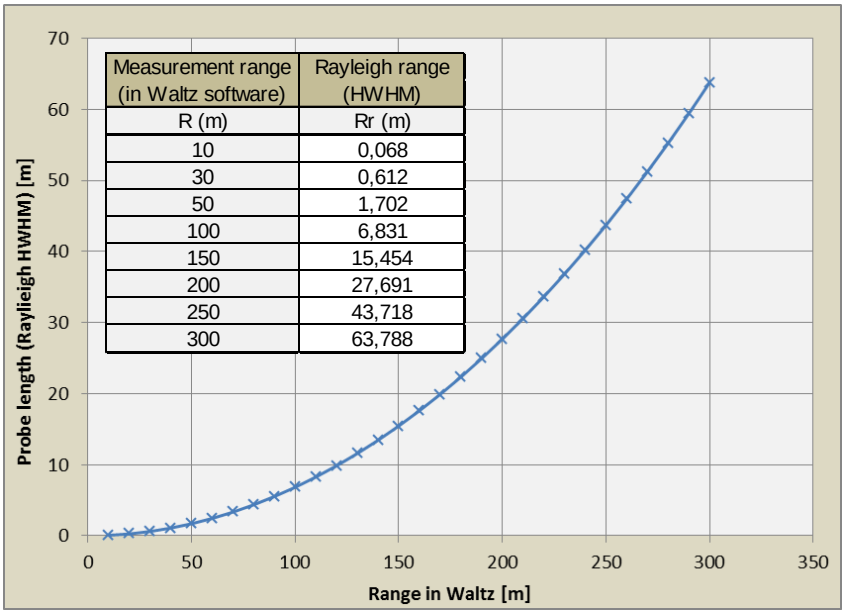

Figure 4. Probe length model of ZDM lidar

The ZDM lidar features a single "scanning" beam. The optical chain from the laser source to the telescope is the same independently of the azimuth position – only the position of the prism differs. Therefore, the calibration of the LOS velocity is performed by computing averages of LOS velocities contained in a single azimuth sector (see 3.3.1).

1.2.3 Recorded measurement data

The ZDM lidar provides 10-minute statistics, reconstructed wind parameters over one revolution (referred to as realtime measurements), and high-resolution raw data. Three levels of data can be distinguished:

- **Raw realtime data** ("RAW_xxx.ZPH" files):
  - at ~50Hz
  - timestamps, rain, azimuth position (0° is the top of the scan, clockwise orientation), LOS velocity, tilt and roll inclination angles, etc.
- **Realtime reconstructed parameters** ("WIND_xxx.ZPH" files obtained with ZephIR's software *Waltz – version v4.449*)
  - at ~1Hz, for one measurement range[2]
  - Raw measurements:
    mean "left" and "right" LOS velocities at speficic heights, tilt and roll inclination angles, fore-aft velocity, etc.
  - Fit- derived (FD) wind parameters:
    e.g. horizontal wind speed (HWS) at scan centre, yaw misalignment, shear exponent.
  - Pair-derived (PD) wind parameters at different heights a.g.l.:
    e.g. yaw misalignment and HWS at hub height.
  - Meteorology station data:
    temperature, pressure, humidity, etc.

[2] If the lidar is configured with multiple ranges, the ~1Hz reconstruction corresponds to the realtime measurement range, i.e. is performed at the "live" range and until the lidar refocuses to the next range.

- **10-minute statistics and 10-minute reconstructed parameters** ("WIND10_xxx.ZPH" files obtained with ZephIR's software *Waltz – version v4.449*)
    - Meteorology station data:
      Temperature, pressure, humidity, etc.
    - Raw measurements:
      Statistics of tilt and roll inclination angles, fore-aft velocity, etc.
    - For each range
        - Fit-derived wind parameters statistics
        - Pair-derived wind parameters statistics
        - For each height:
            - Statistics of "left" and "right" LOS velocities
            - Pair-derived after computing (PDAC) wind parameters: the parameters are computed using 10-min averages of other data. E.g. HWS, turbulence intensity, yaw misalignment.
        - PDAC wind parameters: shear exponent, linear vertical shear and veer, rotor-equivalent wind speed, relative wind direction.

For the calibration of the Radial Wind Speed (RWS) – also called LOS velocity –, 10-minute averages of raw realtime data are created via the SQL database (see 3.3.1).

1.3 Choice of calibration method

The calibration of the ZephIR Dual Mode lidar unit 351 (ZDM351) was performed using the "white box methodology" detailed in [3]. The white box approach consists in calibrating the input quantities of the lidar's reconstruction algorithms rather than calibrating each reconstructed wind parameter – referred to as the black box methodology.

For the ZDM lidar, these inputs are the geometry of the lidar's scanning pattern – i.e. cone angle –, the tilt and roll inclinometers measurements and the LOS velocity.

1.4 Timeline of events

ZDM351 has been calibrated at DTU Wind Energy's test site for large wind turbines between February 2015 and April 2015. The timeline of the main events is (time synchronisation to GMT+1):

- **Inclinometers calibration** (tilt and roll) and **geometry verification** – *2015-02-03* and *2015-02-04*
- Lidar installation (see Figure 14) on *2015-02-05 09:00*
- **LOS velocity calibration**
    - Theodolite measurements, beam positioning and detection using cup anemometer as moving hard target (see 3.2), ranges configuration on *2015-02-05* and *2015-02-06*
    - Valid measurement period: *[2015-02-06 13:00 ; 2015-04-20 12:00]*
- **Decomissioning**
    - Beam position check at *2015-04-20 15:09*
    - Hard target & measurement range test on *2015-04-20 15:00*

Chapter 2

2 Inclinometers calibration and geometry verification

This section concerns the calibration of the tilt inclinometer of the ZephIR Dual Mode lidar. The procedure is detailed together with the obtained results. The section also provides the geometry verification since this was performed prior to the tilt calibration with a similar setup.

2.1 Principles

The internal tilt inclinometer is calibrated by comparing the lidar tilt readings with reference quantity values obtained by: detecting the beam at multiple positions along the scanning pattern (circle) measuring their 3D coordinates in an arbitrary reference frame; transforming the coordinates to the lidar's frame; applying fitting techniques.

In practice, we are only interested in the height difference and horizontal distance between the beam position and the origin of the beam.

2.1.1 Defining the zero axes of inclination

The zeroes of the internal inclinometers are defined (by us, the calibration institute) as:

- $0°$ tilt when the lidar optical centreline is horizontal. The optical centreline is the line between the origin of the beams (apex of the cone) and the center of the circular beam pattern (at one range).
- 0° roll when the line between the two "side" points ($90°$ and $270°$ azimuth) of the circular scanning beam pattern is horizontal.

The definition of the zero axes of inclination is based on the beam's position. In practice, they relate to the manufacturer's definition[3].

[3] We, at DTU Wind Energy, who performed the testing, arbitrarily chose these definitions. Note that the manufacturer's definition (*ZephIRt LiDAR*) is based on heat sink located at the back of the lidar, which is mounted on the same frame as the optical components. In-house, the inclination sensor's voltage characteristics (gain and offset) are adjusted using a "moving belt" test and the heat sink as a reference position.

2.1.2 Measurement setup

The measurement setup (Figure 5) is composed of:

- The ZDM lidar unit
- A fine-tuning tilting system (to be mounted on the rear leg)
- One tall frame (~4m high)
- One long boom, used to find the plane perpendicular to the optical centreline
- One moving hard target of relatively small size; e.g. a cup anemometer can conveniently be used
- One range-finding theodolite ('total station'), providing 3D coordinates (N, E, Z) measurements (see Figure 5). The theodolite is levelled, thus the Z coordinate is in a vertical axis. The axis N and E are orthogonal and define a horizontal plane passing through the origin of the theodolite reference frame
- One computer connected to the lidar for live observations of the lidar responses (determining when the beam is hitting the moving target).

Figure 5. Left: photograph of the measurement setup for ground calibration of the ZephIR Dual-Mode tilt inclimometer. Top right: cup anemometer used as moving hard target. Bottom right: 3D coordinates measurements with a theodolite

Figure 6 and Figure 7 show additional details on the measurement setup:

- The distance between the lidar and the frame should be as large as possible in order to minimise the uncertainty in the tilt angle measurements. The measurement distance is however limited by the range of tilt angles to calibrate and by the height of the frames. Here the distance was ~10m.
- The position of the theodolite has little importance. An adequate position ensures that all the points of interest are measurable (without moving the theodolite). Typically, it can be placed approximately 10m behind frame.

  Note 1: although the ZDM is a class 1 laser product, it is important that the theodolite is placed in an area where it cannot come into contact with the lidar beam, as the magnifying effect of the theodolite lens could cause eye safety issues.

  Note 2: in the case of ZDM351, the theodolite has first been aligned with the Visible Laser Alignment system (VLA), see 2.3.2.1.

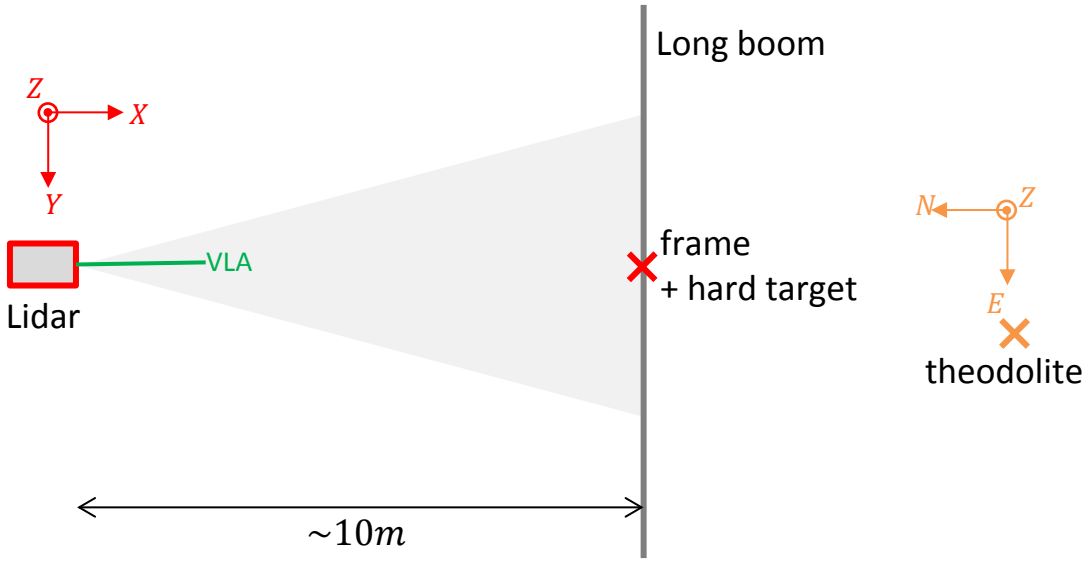

Figure 6. Top-view schematic of the measurement setup for geometry verification and tilt inclinometer calibration

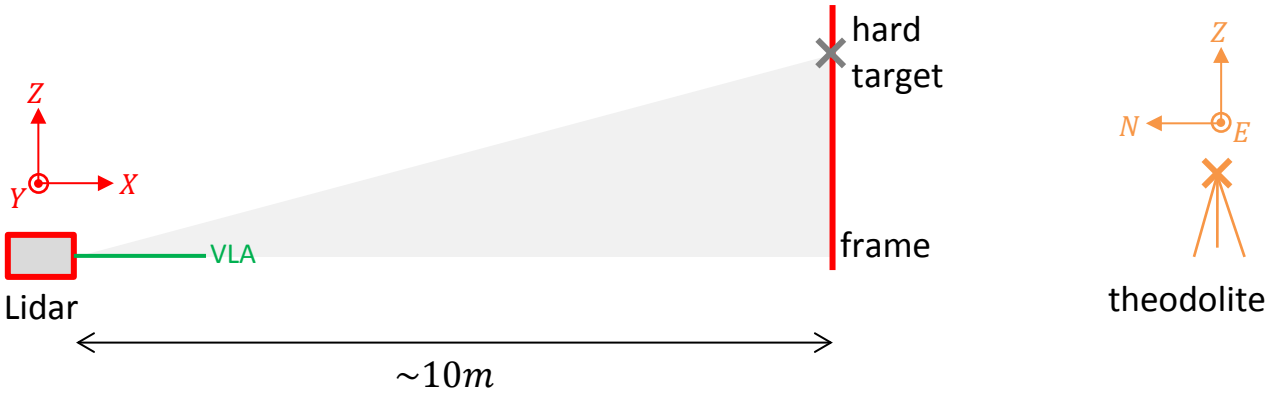

Figure 7. Side-view schematic of the measurement

2.1.3 Accurately detecting the beam position

The beam position is detected by progressively moving the hard target (up and down) until it blocks the beam. When the lidar beam hits the hard target, a high backscatter strength signal can be observed using the "figure of eight" plot: Figure 8 shows the response of the ZDM lidar when its beam hits the moving hard target at the top (left plot) and on a side part of the scanning pattern (right plot); red fading colours correspond to the backscatter signal from the atmosphere.

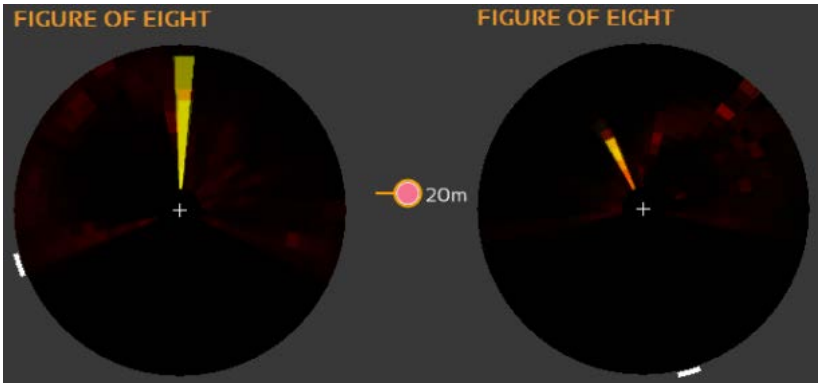

Figure 8. Response of the ZDM when its beam hits a moving hard target

A reference point located on the cup anemometer is physically marked and used to measure the beam position. The physical location of the lidar beam is $20cm$ higher than the marked point (a correction of the measured height or Z-coordinate is applied).

During the ground-testing, the lidar was configured with a single measurement range of 20m.

2.2 Roll verification

In the situation where the ZDM is turbine-mounted, knowing accurately the beam position depends less on the roll than the tilt inclination angles. The roll inclination angle thus plays a minor role in the reconstruction algorithms compared to the tilt. Additionnally, it is practically complex and time-consuming to calibrate the roll inclinometer using beam detection's techniques.

Consequently, a formal calibration of the roll inclinometer has not been performed. Instead, the gain of the roll inclinometer has been verified prior to the deployment by:

- Placing the lidar in ~10 different positions, at $\sim 0°$ tilt and roll in the $[-8°;\ +8°]$ range.
- Measuring the roll angle via the inclinometer of a range-finding laser instrument positioned on the heat sink of the ZDM lidar.
- Comparing the lidar's indicated roll with the measured values

Figure 9 shows the results of the verification test of the roll inclinometer's gain (unforced regression, $R^2 = 0.99996$). The obtained gain value of 0.9991 corresponds to a difference of less than 0.1% compared to the reference instrument.

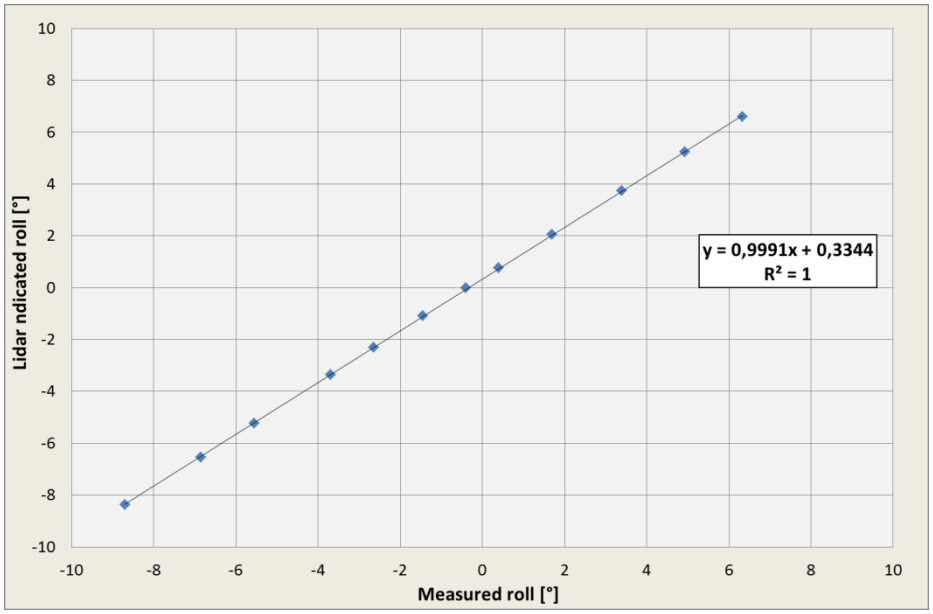

Figure 9. Verification of the roll inclinometer gain

Further, the lidar indicated roll angle $\psi_{indicated}$ will be used without correction.

2.3 Geometry verification

2.3.1 Procedure

The geometry verification is performed by locating the beam at multiple positions along the scanning pattern, at ~0° tilt (lidar reading). For the scanning pattern to be a circle, the measurements must be taken in a plane orthogonal to the lidar optical centreline.

The main steps of the geometry verification are:

1) Alignment of a long boom perpendicular to optical centreline: the Visible Laser Alignment (VLA) system integrated in the lidar is first used as reference. Theodolite measurements of the laser light position (two points) and of the boom (two points) are performed and repeated until the boom marks the plane orthogonal to the centreline.

2) Measurements of the scanning pattern: 10-12 points located on the scanning pattern are measured (N, E, Z). The bottom part of scanning pattern is not measurable (light hitting the ground). Thus, only the top part of the scanning pattern is measured.

3) Measurements of the lidar's window: the geometry of the window is measured (4 red crosses in Figure 10) and coordinates of its center are retrieved. The window's center is considered to relate directly to the "origin of the beam" located inside the pod.

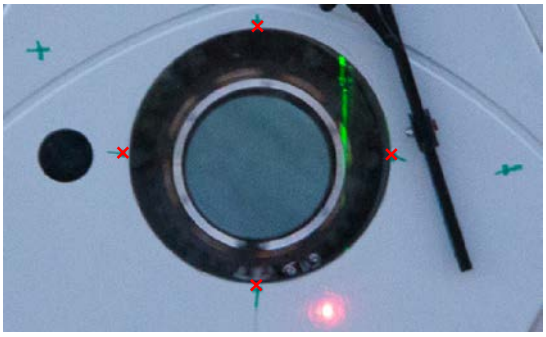

Figure 10. Measuring the geometry of ZDM lidar's window

4) Transforming the 3D coordinates: into a coordinate system based on the lidar's window measurements (see Figure 6, $(N, E, Z) \rightarrow (X, Y, Z)$). The theodolite's reference frame is somewhat arbitrary, with the Z coordinate pointing upwards. The new reference frame (X, Y, Z) is defined by: origin at $(N_{ref}, E_{ref}, Z_{ref})$; X defines the optical centreline direction; the (Y, Z) plane is orthogonal to the optical centreline.

5) Fitting the measured beam location points (Y, Z coord.) to a circle. The fitting results are the coordinates (Y_c, Z_c) of the circle's center and the radius of the circle.

6) Finding the VLA alignment: the y-coordinate Y_c of the circle's center must be ≈ 0.

7) If needed, re-align the long boom and the total station. Then repeat steps 1-6 until $Y_c \approx 0$.

8) Derive the cone angle

2.3.2 Geometrical development

2.3.2.1 Alignment and VLA measurement

During the ground calibration, the theodolite frame of reference (N, E, Z) was first configured so that the N-axis and the lidar VLA are aligned. The first set of beam positions measurements was taken at a distance of ~10m and fitted to a circle which center showed to be $11\ cm$ off (in the Y direction). The optical centreline, i.e. the axis of the conical scanning pattern, was thus slightly misaligned with the VLA, by an angle of: $\text{atan}(0.11/10.05) \approx 0.6°$. This misalignment is compatible by the ±1° manufacturer specified accuracy of the VLA.

In a second step, the theodolite was moved by the found offset and the measurements repeated (see results in 2.3.3).

2.3.2.2 Orthogonality of the (Y, Z) plane

The orthogonality of the (Y, Z) plane to the optical centreline (VLA) can be verified by calculating the dot product between the normalised vectors along the VLA and between two points located on the scanning pattern.

For example, (N_1, E_1, Z_1) and (N_2, E_2, Z_2) being the coordinates of the two measured VLA points, the normalised vector $(N_{VAL,n}, E_{VAL,n}, Z_{VAL,n})$ along the VLA is derived:

$$(N_{VAL}, E_{VAL}, Z_{VAL}) = (N_2, E_2, Z_2) - (N_1, E_1, Z_1)\ ;\ (N_{VAL,n}, E_{VAL,n}, Z_{VAL,n}) = \frac{(N_{VAL}, E_{VAL}, Z_{VAL})}{\sqrt{N_{VAL}^2 + E_{VAL}^2 + Z_{VAL}^2}}$$

The normalised vector between the two points on the scanning pattern being $(N_{scp,n}, E_{scp,n}, Z_{scp,n})$, we calculate the dot product[4] $(N_{scp,n}, E_{scp,n}, Z_{scp,n}) \cdot (N_{VAL,n}, E_{VAL,n}, Z_{VAL,n})$ which should be close to 0.

For ZDM351, the orthogonality has been verified for 5 different pairs of points: dot product absolute values were < 0.01, corresponding to angles of $90° \pm 0.5°$.

2.3.2.3 Circle fitting technique

The circle fitting technique employs an orthogonal distance regression algorithm in two parts: a first estimation of the circle center and radius using QR factorisation is performed ("circfit.m" Matlab code) in order to provide inputs to the non-linear least-squares regression algorithm (developed by NPL Center for Mathematics and Scientific Computing; link).

2.3.2.4 Transformation of coordinate system

The transformation of the coordinate system can be performed numerically (rotation of the system + translation of center) or physically by placing the theodolite on the optical centreline direction and re-aligning its coordinate system (so that the axes of both systems (N, E, Z) and (X, Y, Z) are parallel, i.e. N parallel to X, etc).

[4] The dot product of normalised vector takes values in the $[-1; +1]$ range. 0 indicates perfect orthogonality, +1 or -1 indicate collinearity.

The later option was chosen for the ground testing of the ZDM unit 351 lidar. Additionally, $57mm$ offset was applied on the horizontal distance (X axis) corresponding to the distance between the prism (origin of the beam) and the window (see Figure 10).

2.3.3 Results

Figure 11 shows the measurement points of the ZDM lidar beam pattern and the fitting results. As required, the center coordinate $Y_c \approx 0$.

The radius is $R_{fit} = 2.68m$. The X coordinate of the center has been measured to $X_c = 10.103\,m$ (on average with a standard deviation between the points of $stdv\,(X_c) = 0.015m$). Thus the measured cone angle is $\alpha_m = \text{atan}\left(\frac{R_{fit}}{X_c}\right) \approx 14.86°$, reasonably close ($-0.11°$) to α_{th}.

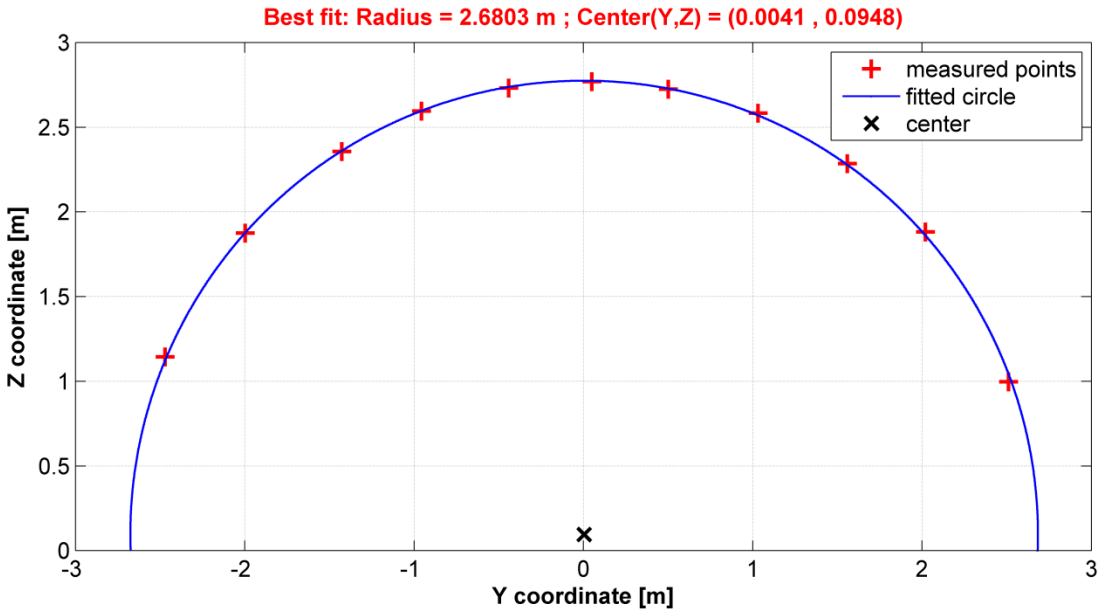

Figure 11. Circle fitting of the ZDM lidar beam pattern for cone angle verification

2.4 Tilt calibration

2.4.1 Procedure

The tilt calibration has been performed by:

- Placing the lidar in ~10 different tilt configurations, in a range of approximately ±3°;
- For each tilt configuration:
  - Locating the beam at the top of the circular pattern (i.e. at $Y \approx 0$) and measuring its position (N, E, Z);
  - Measuring the position of a reference point on the window and deriving the coordinates of the center $(N_{ref}, E_{ref}, Z_{ref})$
  - Deriving the beam tilt angle $\varphi_{beam} = \text{atan}\left(\frac{Z - Z_{ref}}{\sqrt{(N-N_{ref})^2 + (E-E_{ref})^2}}\right) = \text{atan}\left(\frac{\Delta Z}{D_{ref}}\right)$
  - Deriving the lidar tilt angle by $\varphi_{meas} = \varphi_{beam} - \alpha_{th}$
- Plotting the measured tilt angle φ_{meas} against the lidar indicated tilt $\varphi_{indicated}$ and performing a linear regression.

2.4.2 Results

The tilt calibration results are presented in Figure 12. The retained calibration relation is the unforced linear regression:

$$\varphi_{BE} = 0.9901 \cdot \varphi_{indicated} + 0.3856°$$

where φ_{BE} is the best estimate of the tilt angle, i.e. the calibrated tilt angle obtained by correcting the lidar indicated tilt $\varphi_{indicated}$.

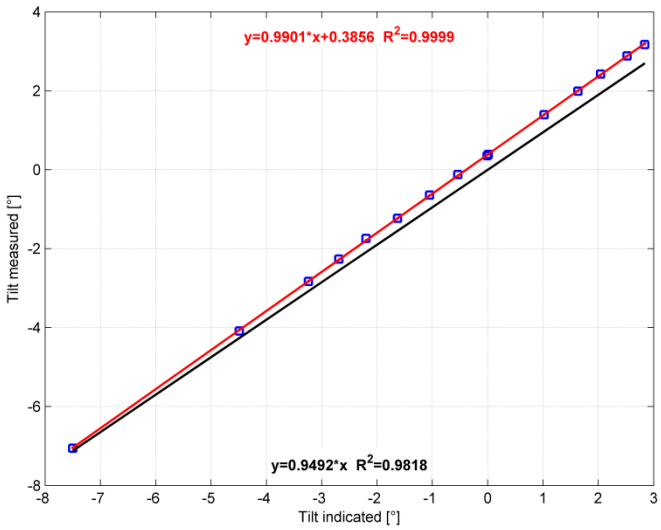

Figure 12. Tilt calibration results: measured vs. lidar indicated

The calibration is incomplete if the measurement uncertainty is not specified (cf. metrological definition in [5]). The tilt calibration uncertainties are derived using the GUM methodology (see [6]) and detailed in Annex A. The uncertainty on φ_{BE} with a coverage factor of 2 is: $U_{\varphi_{BE}} = 0.16°$.

Chapter 3

3 RWS calibration

This section describes the measurement setup of the RWS calibration of the ZDM unit 351 lidar and provides the calibration results of the radial wind speed (RWS) – also called LOS velocity.

3.1 Measurement setup

3.1.1 Measurement systems

The measurement setup providing the required data of the RWS calibration campaign is:

- Reference instruments (Figure 13):
  - top-mounted on two met. masts distant by $5.3m$ at height a.g.l. $H_{mast} = 8.9m$.
  - one cup anemometer: to measure horizontal wind speed, type Thies First class advanced (see calibration certificate in Annex B and classification in [7]).
  - one sonic anemometer: to measure wind direction, type Gill 1210R3-50 (see calibration certificate in Annex C).

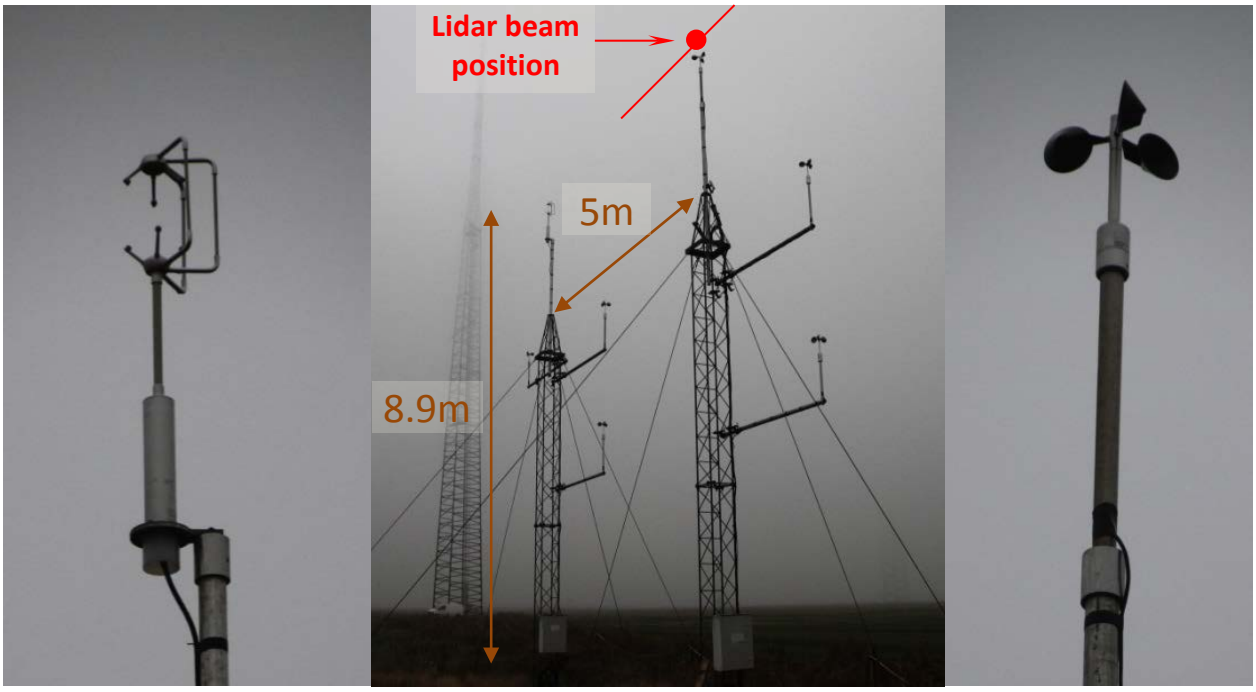

Figure 13. Reference instruments for RWS calibration: sonic anemometer (left), two masts (center), cup anemometer (right)

- ZDM lidar mounted on its three legs + fine tilting adjustment system (Annex D) and placed on stable ground (see Figure 14)
  - ~262m from the reference instruments. The terrain between the lidar and the masts is a flat open field.
  - the tilting is adjusted until the bottom part (azimuth = 180°) of the beam pattern is located at the height of the reference instruments. The resulting physical[5] tilting was measured using the total station to:

$$\varphi_{physical} = \text{atan}\left(\frac{H_{mast} - H_{lidar}}{D_{physical}}\right) \approx 1.65° \qquad \text{(eq. 1)}$$

Figure 14. Calibration measurement setup of the ZDM lidar at DTU Wind Energy test site, Høvsøre (DK)

3.1.2 Range configuration

The distance between the lidar and the cup anemometer – i.e. the main reference instrument – has been measured to $D_{cal} = 261.8m$ using the theodolite. The lidar measurement range is defined along the optical centerline. Thus, the measurement range for the calibration is $D_{cal} \cdot \cos \alpha_{th} = \mathbf{253\ m}$ and corresponds to the configured range in the ZDM lidar's software ("Waltz").

[5] Physical as opposed to the lidar reading of the tilt inclination, based on the optical centerline.

3.1.3 Reasons for choosing the Høvsøre measurement setup

The two met. masts were initially installed for previous research projects. Developing the procedures and performing calibrations using reference instruments mounted on these masts was convenient. Even though the measurement setup is certainly not optimal, it is suitable for the RWS calibration of nacelle lidars and provide the necessary data. The reasons for using the described measurement setup (3.1.1) are:

- Site location and characteristics: Høvsøre is located on the West coast of Jutland in Denmark, ~2km from the sea and the terrain is flat.

- Wind climate: strong westernly winds coming from the North Sea are typical (Annex E). Consequently, the calibration can be completed faster since filling in high wind speed bins is usually the most time-consuming part of the calibration.

- Height of the two met. masts: nacelle lidars should be calibrated in conditions similar to the operational ones. However, measuring at typical modern wind turbines' hub height (~ 80-100m) is in practice difficult. The lidar would need to be placed on a stiff platform to avoid measurement uncertainties due to the tilting and rolling of the structure (see [4]). At such heights, stiff structures (e.g. concrete) are extremely expensive. Thus, the height of 10m was preferred and more suitable since the lidars could, at first, be placed on a 10m platform in a mast, so that the beam is horizontal while being calibrated. Placing the lidar on the ground with its beam tilted up is a valid alternative, as demonstrated in [3] and this report. On the negative side, the 10m height a.g.l. implies relatively high turbulence which is known to impact reference anemometers (e.g. cups). Consequently, the ideal setup would have to compromise between measuring at greater heights and limiting the tilting of the beam.

- Measurement distance: one of the main applications of profiling nacelle lidars is the measurement of power curves. Standards in power performance ([8]) currently require the wind to be measured at a distance eauivalent to 2.5 rotor diameters – i.e. 250-300m for modern wind turbines. The measurement distance of ~260m in the calibration setup fits well these requirements. Additionally, it allows testing nacelle lidars close to the limits of their current measurement range capabilities.

- Reference instruments: for decades, the wind industry mainly relied on cup anemometers and wind vanes for wind speed and direction measurement. Current standards specify ([8]) how to assess the uncertainty of cup anemometers. Sonic anemometers seem like a viable alternative although their operational measurement uncertainty is not yet thoroughly implemented in standards. We chose to rely on two reference instruments – one cup anemometer for wind speed (main driver of (eq. 5)), and one sonic for wind direction – rather than only a sonic anemometer. Both are affordable instruments.

- Two masts or one? Both reference instruments are top-mounted on their respective mast in order to prevent mutual flow perturbation, and to minimise mounting uncertainties. However, one could also consider using only one mast and alternative mounting techniques allowing the two instruments to measure at the same height.

3.2 Beam positioning technique

The employed positioning technique makes use of a moving hard target – the top-mounted cup anemometer – similarly to 2.1.3. The ZDM lidar is placed at ~0° roll and the tilting adjusted until the bottom part of the beam pattern is known to hit the hard target (azimuth =180°). Figure 15 shows the response of the ZDM lidar when the cup anemometer is hit (left) and stopped from rotating (right) at a distance of 262m.

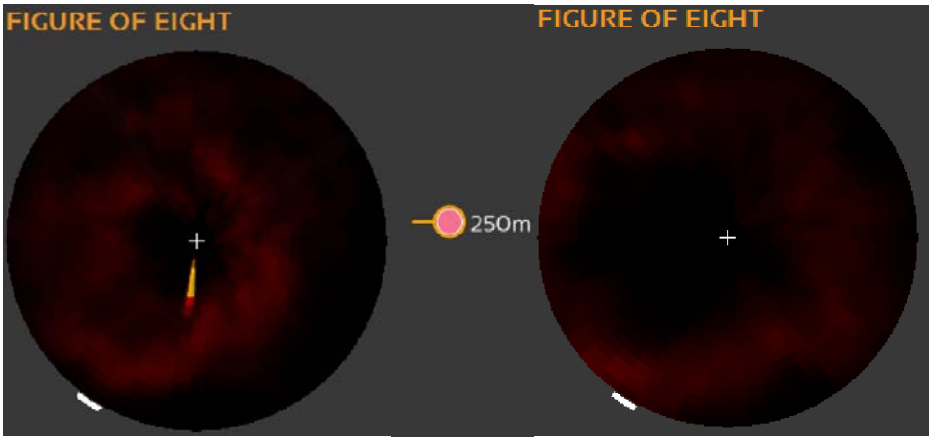

Figure 15. Positioning the bottom part of the ZDM beam pattern close to the reference anemometer

Once the beam is detected to hit the cup anemometer, the lidar is tilted up by ~0.02° to avoid contamination of the LOS velocity estimation by the tangential velocity of the cup anemometer. With the described measurement setup, 0.02° corresponds to a height offset of $10cm$.

3.3 Data analysis

3.3.1 Deriving the averaged RWS

The averaged RWS at the bottom of the scan is not provided by the lidar's firmware. It is derived from the RAW data (see 1.2.3) by averaging the fast data when the reported azimuth angle – also called phase – is within a narrow sector chosen to be $[179° - 181°]$.

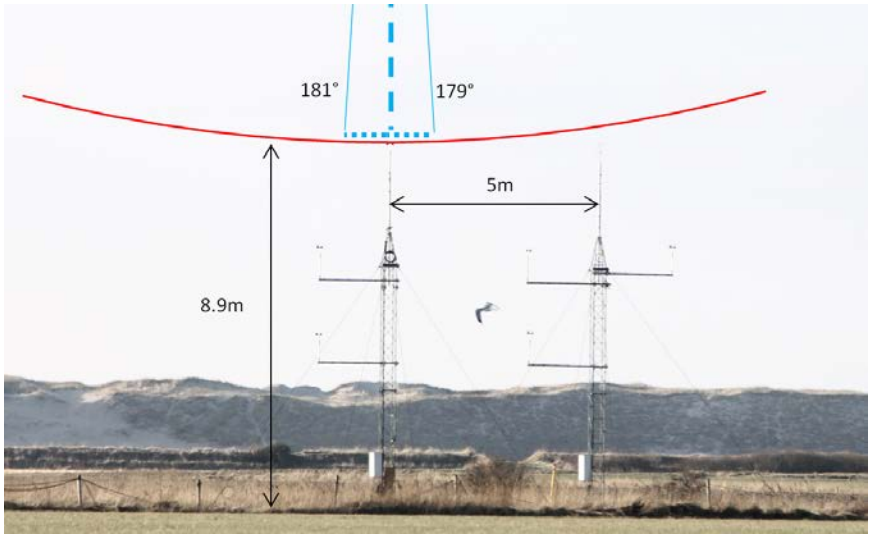

Figure 16. Averaging LOS velocity measurements in a narrow azimuth sector (ZDM lidar)

Annex F provides the query used to create the averaged table of raw data in a SQL database.

A potential issue here is that the averaging of the LOS velocity relies on the azimuth angle reported by the lidar. In other words, when the ZDM lidar reports 180° aximuth, it must correspond to the lowest point of the scanning pattern. Figure 15 shows that the lidar seems to report consistent azimuth values (macro indication of the correctness). Additionally, the LOS direction obtained in 3.4.2 is consistent with the values obtained from another lidar being calibrated simultaneously (difference in LOS direction < 1.5°), which would not be the case if the reported azimuth angles were incorrect.

3.3.2 List of data

The list of data used in the analysis and filters is given below. Note: the data listed below in ⟨ ⟩ are based on 10-minute statistics.

Table 1. List of data for RWS calibration analysis

Symbol	Unit	Description (instrument)
$\langle HWS \rangle_{vec}$ or $\langle HWS \rangle_{vec,\ cup}$	m/s	Vector mean horizontal wind speed (cup anemometer)
$\varphi_{physical}$	deg	Physical lidar tilt angle: measured using the theodolite to $1.65°$. (theodolite)
$\langle \theta \rangle_{vec}$	deg	Vector mean horizontal wind direction (sonic anemometer)
$\langle HWS \rangle_{vec,\ sonic}$	m/s	Vector mean horizontal wind speed (sonic anemometer)
$\langle \varphi_{flow} \rangle$	deg	Flow tilt angle (sonic anemometer)
LOS_{avail}	-	"Availability" of the LOS velocity within the chosen azimuth sector: $LOS_{avail} = \frac{number\ of\ valid\ data\ points}{maximum\ number\ of\ points\ in\ 10min}$
$StatA_{sonic}$	-	The status address is a binary result message, generated at the sonic sampling frequency (i.e. 20 Hz)

Notes:

- Due to low-pass filtering of the inclinometers' measurements by the ZDM's firmware (nacelle motion purposes), a fixed value is used for the entire calibration period instead of the lidar indicated tilt $\varphi_{indicated}$. The fixed value is equal to $\varphi_{physical}$ (see 3.1.1).
- One revolution is performed every second, i.e. 600 in 10 minutes. $LOS_{avail} = \frac{number\ of\ valid\ data\ points}{600}$. However, the chosen azimuth sector is $2°$ wide, while one phase sector is $\approx 360/48.8 = 7.38°$ wide. In a 10min period, the expected maximum "availability" of the LOS within the azimuth sector is:

$$\frac{2°}{360°/48.8} \approx 0.271$$

3.3.3 Filters

The valid dataset of 10-min averaged data is obtained by filtering as follows, except for the LOS direction estimation using the fitting technique (3.3.4.1) for which the wind direction filter is not applied:

- Vector mean HWS from cup anemometer:
  - $\langle HWS \rangle_{vec} \in [4\,;16]\ m.s^{-1}$
  - corresponding to the calibrated range of HWS.
- Check of HWS validity
  - $abs\left(\langle HWS \rangle_{vec} - \langle HWS \rangle_{vec,\ sonic}\right) < 0.3\ m.s^{-1}$
  - Unpredictable reference measurement accidents yielding outliers are removed, e.g. a bird sitting on sonic anemometer.
- Flow tilt:
  - $\langle \varphi_{flow} \rangle \in [-2°\,;\ 2°]$
  - to limit the contribution of the wind vector's vertical component to the RWS, that is neglected in the RWS calibration (see 3.1 in [3]).
- LOS availability:
  - $LOS_{avail} > 0.2.$
  - Good data availability is required in order to reduce potential biases due to failed measurements. Note that 0.2 corresponds to an availability of $\sim 75\%$ compared to the theoretical maximum value (see 3.3.2)
- Sonic status address (bit number)
  - $\min(StatA_{sonic}) \geq 01.$
  - $StatA_{sonic} = 00$ indicates error codes. Thus, the 10-min period is filtered out if one 00 value is found.
- Wind direction:
  - $\langle \theta \rangle_{vec} \in LOS_{dir} \pm 40°$
  - Filter with respect to the preferred measuring direction of the lidar, and due to the asymmetry of the sonic anemometer probes. The ±40° sector replicates operational conditions for which nacelle lidars are designed, i.e. flow towards the lidar, and reasonable yaw misalignment of the turbine (not likely to reach a value as high as 40°).
  - Filter only applied starting from step 3.5.4.2.

3.3.4 LOS direction evaluation

The LOS direction evaluation follows the two-step process described in [3].

3.3.4.1 Wind direction response fitting – approximate LOS_{dir}

The response of the normalised lidar RWS to the wind direction is fitted to a rectified sine wave. The RWS ($\langle RWS_{norm} \rangle$) is normalised by the cup anemometer HWS projected only in the vertical plane:

$$\langle RWS_{norm} \rangle = \langle RWS \rangle / \left(\langle HWS \rangle_{vect} \cdot \cos\langle \varphi_{physical} \rangle \right) \qquad \text{(eq. 2)}$$

The fitting function is obtained using the method of least squares:

$$f_{fit}(\langle \theta \rangle_{vec}) = a_{LOS} \cdot |\cos(\langle \theta \rangle_{vec} - \theta_0)| + b_{LOS} \qquad \text{(eq. 3)}$$

Consequently, three parameters are obtained from the fitting process, i.e. the gain a_{LOS}, the offset b_{LOS}, and the approximate LOS direction θ_0. The gain and offset are only indications of the data quality and expected to be close to respectively 1 and 0. θ_0 is further used in 3.5.4.2.

3.3.4.2 Residual sum of squares (RSS) – accurate LOS_{dir}

To refine the estimation of the LOS direction, the so-called RSS process is applied. The dataset of 10-min averaged data is restricted to wind directions in the range $\theta_0 \pm 40°$. Linear regressions are then performed between $\langle RWS \rangle$ and the reference wind speed projected using angles θ_{proj} contained in the range $\theta_0 \pm 1°$ with a step of e.g. $0.1°$:

$$\langle HWS \rangle_{vec} \cdot \cos\big(\langle \varphi_{physical} \rangle\big) \cdot \cos(\langle \theta \rangle_{vec} - \theta_{proj}) \qquad \text{(eq. 4)}$$

The residual sum of squares (RSS) of each linear regression is reported and plotted vs. θ_{proj} (see Figure 18). A 2nd order polynomial is fitted to the obtained curve. The LOS direction LOS_{dir} is the minimum of the parabola.

3.3.5 Calibration results: linear regressions on raw and binned data

The reported calibration relation results are linear regressions between the RWS and reference measurand $Ref_{eq\ RWS}$, where:

$$Ref_{eq\ RWS} = \langle HWS \rangle_{vec} \cdot \cos\big(\langle \varphi_{physical} \rangle\big) \cdot \cos(\langle \theta \rangle_{vec} - LOS_{dir}) \qquad \text{(eq. 5)}$$

Both forced and unforced linear regressions are performed on the filtered 10-min averaged data ("raw") and on the corresponding binned data. The binning process is:

- $0.5\ m.s^{-1}$ bin width.
- RWS range $[2.75\,;16.25]\ m.s^{-1}$. The minimum bin ($[2.75\,;3.25]\ \mathrm{m.s^{-1}}$) corresponds to the $4 \cdot \cos 40° \cdot \cos 1.65° \approx 3.06\ m.s^{-1}$ value that can be obtained by projecting the mimimum HWS. Similarly, the $[15.75\,;16.25]\ m.s^{-1}$ bin corresponds to the maximum value of $16\ m.s^{-1}$.
- a bin is considered valid if it contains at least 3 data points.

Note: the retained calibration relation is the forced regression of the binned data (see 4.5 in [3]).

3.4 Calibration results

3.4.1 Calibration dataset

The distribution of valid 10-minute averaged RWS data – i.e. after filtering – is plotted (Figure 17). The mean RWS and number of valid data points are given on the top right of the graphs.

The completion criterion for the calibration of one beam is typically that wind speed bins between 4 and 12 m/s are valid (≥ 30min data in bin). However, meeting such a criterion mainly depends on atmospheric conditions – more precisely on the occurrence of high wind speeds from the relevant wind directions – and may sometimes be difficult to achieve.

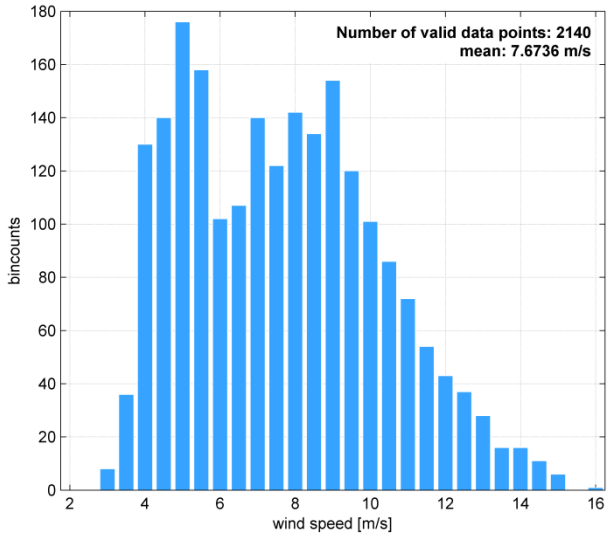

Figure 17. Distributions of radial wind speeds after filtering

3.4.2 LOS direction

Figure 18 shows the results of the two-step LOS direction estimation process, with the fitting coefficients in the top left of the graphs. The final LOS direction is 287.4°.

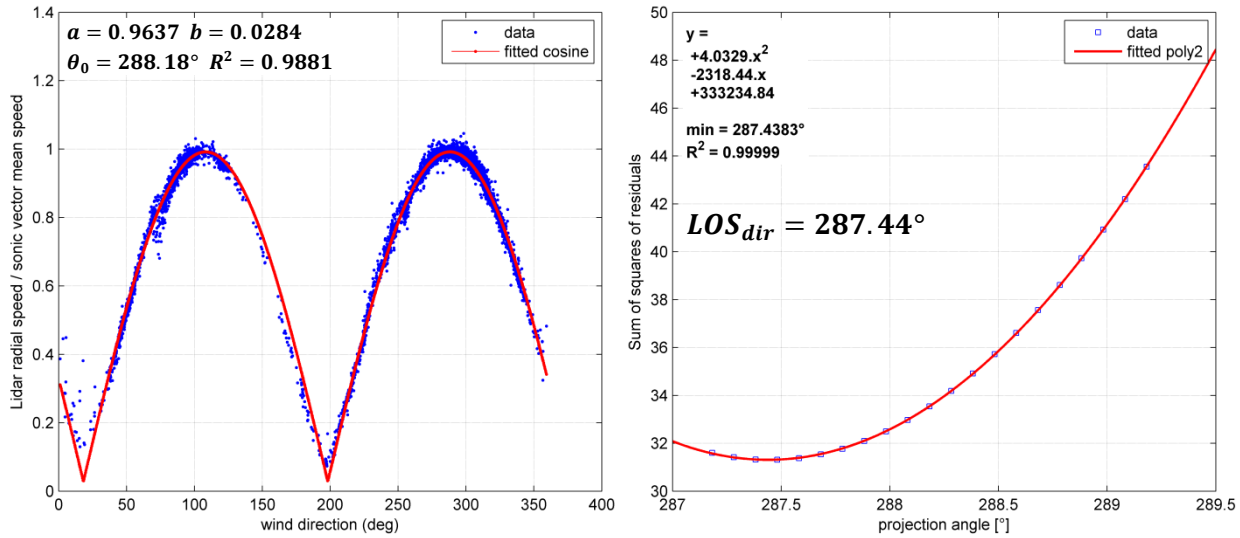

Figure 18. LOS direction evaluation using the rectified cosine fitting (left) and RSS process (right)

3.4.3 Linear regressions

Scatter plots of both raw 10-minute and binned RWS data are shown together with the corresponding forced and unforced linear regression results (Figure 19).

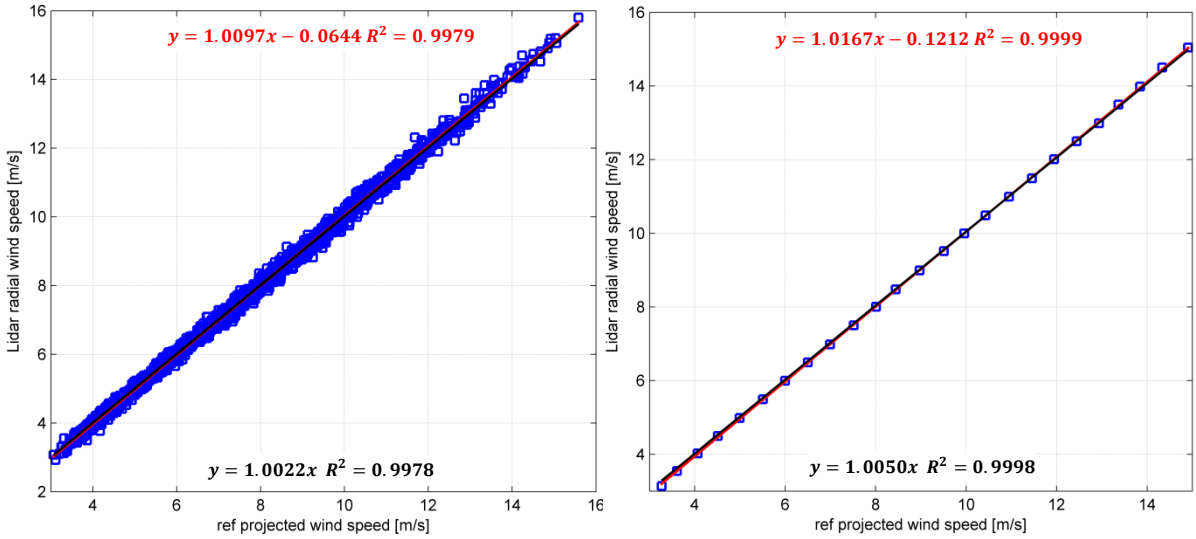

Figure 19. RWS calibration results: 10-minute averaged (left) and binned (right) data

3.4.4 Summary of calibration results

Table 2 summarises the calibration results. **Only the forced regression coefficients on the binned data are given since this corresponds to the selected calibration relation** for the derivation of RWS measurement uncertainties (see 5.7 in [3]).

Table 2. Summary of calibration results – linear regressions (binned RWS vs. reference)

		"2-deg phase" LOS velocity
LOS direction		287.44°
Number of valid data points		2140
Forced regression on binned data	Gain	1.0050
	R^2	0.9998

NB: Annex G provides detailed calibration results tables on both 10-minute and binned data. The results are presented using the cup anemometer for reference wind speed measurements (preferred method). Similar tables obtained by applying the entire calibration using the sonic anemometer only – i.e. both for HWS and wind direction – as reference measurement instrument are provided for information.

3.5 Further investigations

3.5.1 RWS measurement error sensitivity analysis

As explained in [3] (chapter 5.2 "The question of repeatability"), the field calibration of lidars is performed in atmospheric and thus uncontrollable conditions. Based on 10-min averaged data, the influence of external parameters on the RWS measurement error, defined as $\Delta RWS = \langle RWS \rangle - Ref_{eq\,RWS}$, is investigated. The studied parameters are:

- temperature ($T_{abs,2m}$): absolute, measured at 2m a.g.l. on a mast located close to the lidar position ;
- horizontal wind speed $\langle HWS \rangle_{vect}$;
- turbulence intensity: obtained from the reference cup anemometer, $TI = \sigma_{HWS}/\langle HWS \rangle$;
- wind direction $\langle \theta \rangle_{vec}$;
- flow tilt angle: φ_{flow} measured by the reference sonic anemometer ;

Figure 20 displays the results of the sensitivity analysis using the averaged RWS obtained from the ZDM lidar (cf. 3.3.1) in the form of scatter plots of ΔRWS (in $m.s^{-1}$) vs. the aforementioned external parameters.

No significant sensitivity to temperature[6] (a), turbulence intensity (c) or the HWS (b) can be observed. The RWS measurement error seems on the other hand to be slightly sensitive to both the flow tilt angle (e) and the wind direction (d). Indeed, scattered parabolic trends centered respectively on 0° (i.e. horizontal flow) and on ~285° corresponding to the LOS direction can be identified. It is very possible that those sensitivities are due to the cup rather than the ZDM lidar, as similar sensitivities were observed for other lidar units.

[6] Note the low range of temperatures obversed in Figure 20, corresponding to Winter meteorological conditions in Denmark

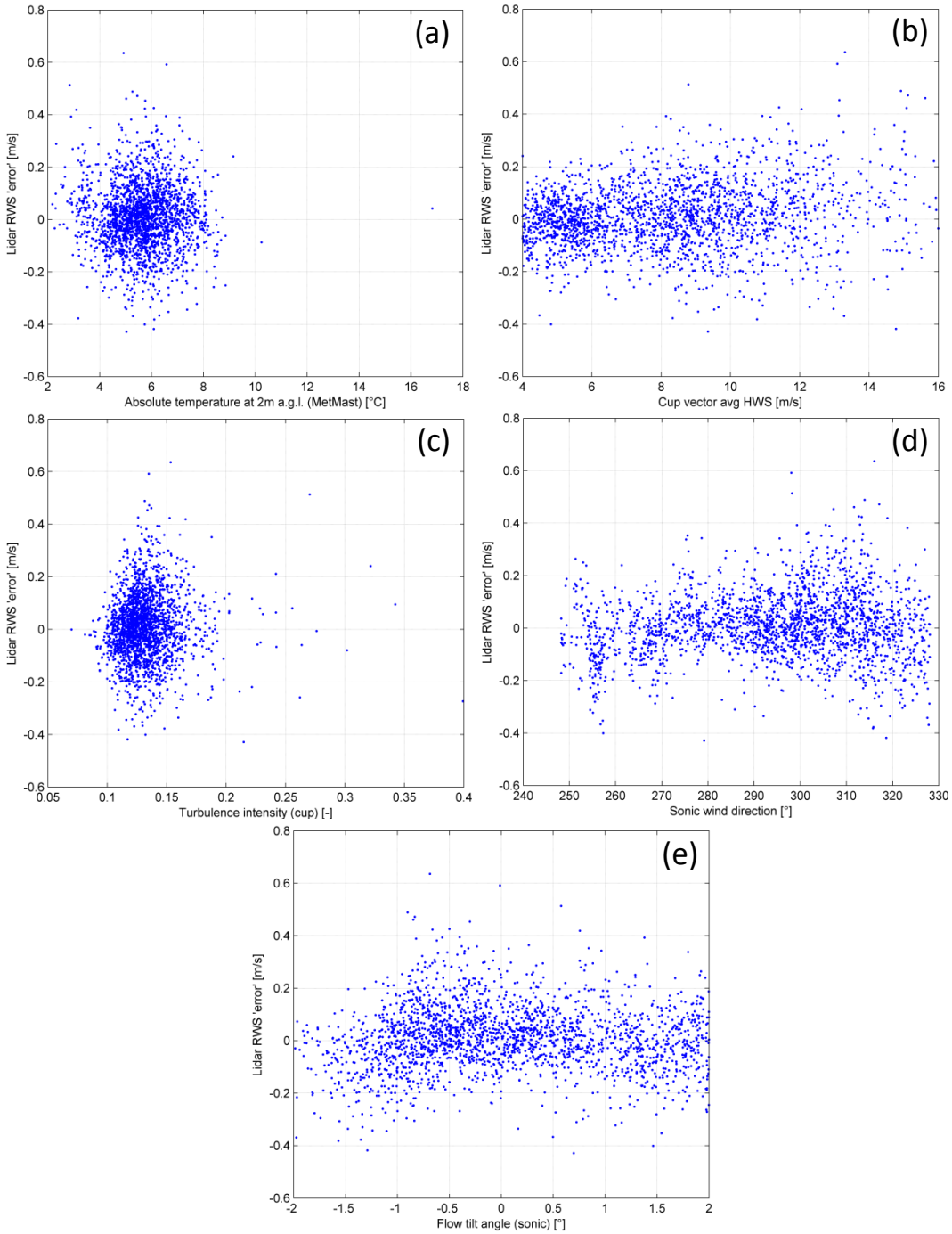

Figure 20. RWS measurement error vs. temperature (a), HWS (b), TI (c), wind direction (d) and flow tilt (e)

3.5.2 Impact of individual filters

Various filters are applied on the 10-minute averaged data before analysis, as detailed in 3.3.3. They impact the quality of the calibration data (outliers detection) and the duration of the data collection. Their impact is analysed by determining the number of points removed (Table 3):

- Individually: only one filter is applied. The proportion of points removed from the unfiltered dataset is derived;
- Sequentially: filters are added one after another. The obtained dataset size is compared to the one at the previous step;
- "Wind direction filter + individually": the wind direction sector of interest is systematically used. Other filters are added individually.

Table 3 shows that the "LOS availability" and "sonic status address" filter out less than 1% of the data and thus have a negligible impact on the data collection. On average, valid wind directions were observed 70% of the time. This filter directly influences the duration of the calibration.

Additionnally, westernly winds typically come at the Høvsøre site with high wind speeds (see Annex E and [9]). The calibrated HWS (4-16 m/s) filter removes roughly 13% of the data for valid wind directions.

The sonic anemometer measurements prove, as expected, to be affected by winds outside of the preferred sector: the flow tilt angle and HWS validity filters remove respectively 44% and 7% of the data when all wind directions are used vs. 13% and 3% in the valid sector.

Note: in the case where the wind direction reference instrument is a wind vane instead of a sonic anemometer, the HWS validity and flow tilt angle filters cannot be applied. These filters have a negligible impact on the calibration results. If no HWS validity filter is applied, the calibration relation results, i.e. the gain on the forced binned data, differ by less than 0.02%. If no flow tilt angle is applied, these results vary by ~0.1%.

Finally, the LOS availability threshold filters out few data points.

Table 3. Filters analysis of the RWS calibration datasets

		Individual		WDir + Individual		Sequential	
	Filter name	pts removed		pts removed		pts removed	
2° phase	Wind direction	6540	70%	-	-	6540	70%
-	calibrated HWS	1647	18%	381	13%	381	13%
unfiltered	Flow tilt angle	4094	44%	367	13%	281	11%
dataset:	HWS validity (outlier detection)	658	7%	91	3%	32	1%
	LOS availability	16	0%	8	0%	6	0%
9380 pts	Sonic status address	6	0%	0	0%	0	0%

3.5.3 Impact of LOS velocity averaging method: width of azimuth sector

In 3.3.1, a 2°-wide azimuth sector was employed to average the LOS velocity. This choice was made in order to minimise the spatial separation between the reference anemometer and the lidar. The impact of the sector width on the calibration results is analysed by applying the same steps of the calibration with different widths of azimuth sector providing the averaged LOS velocity:

Width of sector	2°	4°	6°	8°	10°
Valid phase angles	$[179°; 181°]$	$[178°; 182°]$	$[177°; 183°]$	$[176°; 184°]$	$[175°; 185°]$

The calibration results are reported in Annex G. One can observe that the impact of the valid azimuth sector width used for averaging is negligible: the calibration results (e.g. gain of forced regression on binned data) shows differences of less than 0.1% between the 10° and 2° cases.

Chapter 4

4 Measurement uncertainties

The procedure developed to assess the RWS measurement uncertainties of nacelle lidars is detailed in chapter 5 of [3]. It is based on the GUM methodology (see [6]) and thus relies on the law of propagation of uncertainties.

Consequently, this section only provides the list of uncertainty components, their numeric values employed to derive the RWS measurement uncertainty, and finally the uncertainties results for each LOS.

4.1 RWS uncertainty components

4.1.1 Reference instruments uncertainty sources

The reference instruments are the cup and sonic anemometers, providing the HWS and wind direction respectively. The assessment of their measurement uncertainties follows the latest IEC 61400-12-1 methodology [8].

The uncertainty sources, which values are specified for a coverage factor $k = 1$, are:

- **For the HWS**
  - **Wind tunnel calibration uncertainty (type B)**:

$$u_{cal} = u_{cal\,1} + \frac{0.01}{\sqrt{3}} \cdot \langle HWS \rangle$$

    Where $u_{cal\,1}$ is taken from the calibration certificate (Annex B), $u_{cal\,1} \approx 0.025\ m.s^{-1}$.
  - **Operational uncertainty (type B)**:

$$u_{ope} = \frac{1}{\sqrt{3}} \cdot cup\ class\ number \cdot (0.05 + 0.005 \cdot \langle HWS \rangle)$$

    The calibration has been performed using a "Thies First Class Advanced" cup anemometer (without heating regulation), classified as a class A0.9 anemometer by Deutsche WindGuard. The atmospheric conditions of the A class are compatible with the Høvsøre test site. Thus, the class number we used is 0.9[7].

  - **Mounting uncertainty (type B)**: see Annex G of [8]

$$u_{mast} = 0.5\% \cdot \langle HWS \rangle$$

- **For the wind direction (type B)**: taken from the calibration certificate (see Annex C)

$$u_{WD} \approx 0.4°$$

[7] Alternatively, a class S may be used.

4.1.2 Calibration process uncertainty sources

The uncertainty sources relative to the calibration measurement process are:

- **LOS direction uncertainty (type B)**:

$$u_{LOS\,dir} = 0.1°$$

- **Uncertainty of physical inclination angle (type B)**:

$$u_{\varphi} = 0.16°$$

- **Beam positioning uncertainty (type B)** resulting in wind speed deviations. The positioning uncertainty is conservatively estimated to $u_H = 10\,cm$. This translates at the mast height of $H = 8.9m$ and with a shear exponent estimated – using HWS measurements at different heights - to $\alpha_{exp} = 0.2$ into a wind speed uncertainty of:

$$u_{pos} = \alpha_{exp} \cdot \frac{u_H}{H} \cdot HWS \approx 0.23\% \cdot \langle HWS \rangle$$

- **Inclined beam and range uncertainty (type B)**: estimated in [3] using the probe length of the ZDM lidar at 262m, a range uncertainty of 5m, and the setup of the RWS calibration to:

$$u_{inc} = 0.104\% \cdot \langle HWS \rangle$$

4.2 RWS Uncertainty results

The uncertainty results correspond to the calibration uncertainty of 10-min averaged RWS measurements performed by the lidar infield.

NB: that the calibration uncertainty is not the total uncertainty of the RWS measurements, but only part of it. Once measuring as a stand-alone instrument, additional components may be relevant depending on the operational conditions (e.g. measurements in complex terrain).

The uncertainty results are presented in details using the 2°-wide azimuth sector (see 3.3.1).

4.2.1 Uncertainty assessment methodology

The RWS uncertainty assessment is performed using a procedure based on the forced linear regression between the lidar RWS and reference quantity values (see “option 2a” in [3], 5.4.2). With this method, the best estimate of the RWS is defined, using the reciprocal of the obtained calibration relation, as:

$$\langle RWS_{BE} \rangle = \frac{\langle RWS_{indicated} \rangle}{a_{binned}}$$

Where $\langle RWS_{indicated} \rangle$ is the lidar indicated 10-min average RWS and a_{binned} is the gain of the forced linear regression between the binned lidar RWS and $Ref_{eq\,RWS}$ (see 3.3.4). $y_m = a_{binned} \cdot Ref_{eq\,RWS}$ is the estimated measurand. I.e. y_m defines the measurement model allowing to, following the GUM methodology, propagate the reference instruments uncertainties to the lidar RWS.

4.2.2 Expanded uncertainty results

The expanded uncertainties (coverage factor $k = 2$, i.e. defining a 95% confidence interval) are plotted against the RWS bin averages (Figure 21). The expanded uncertainty varies linearly with the wind speed (or bin number), with a coefficient of determination of $R^2 = 0.9989$.

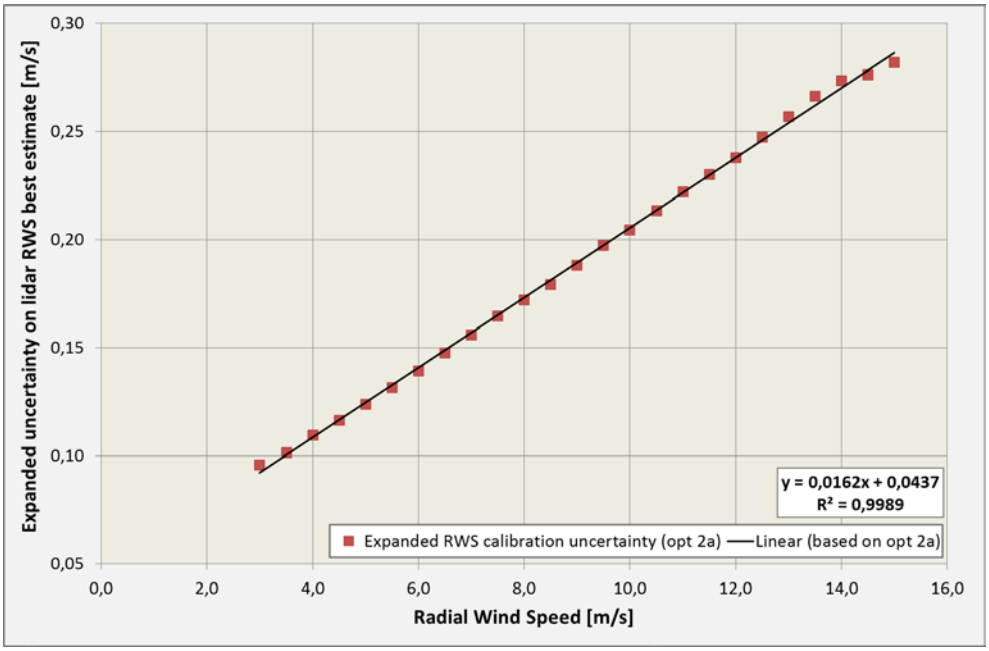

Figure 21. RWS calibration expanded uncertainty (ZDM351)

Figure 22 shows the expanded uncertainty in error bars together with the binned calibration results.

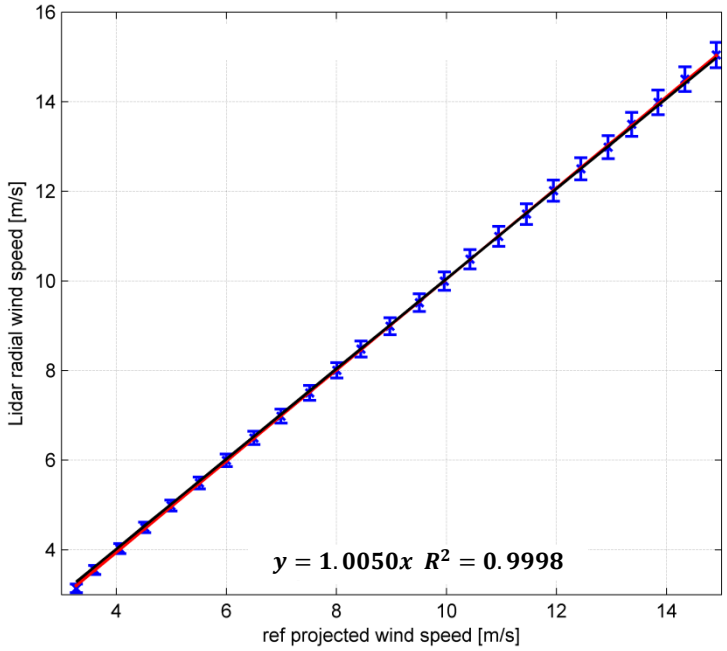

Figure 22. RWS calibration expanded uncertainty results in error bars (ZDM351)

4.2.3 Analysis of uncertainty components

The two tables below provide the values of the uncertainty components used in the uncertainty assessment:

- Table 4:
  - Columns 4-6: uncertainty components contributing to $Ref_{eq\ RWS}$
  - Column 7: combined uncertainty on $Ref_{eq\ RWS}$ (coverage factor $k = 1$)
  - Columns 8-10: uncertainty components contributing and combined uncertainty on y_m. Note that U_{c,y_m} is the total RWS calibration uncertainty ($k = 1$).
- Table 8:
  - Columns 4-8: uncertainty components contributing to $\langle HWS \rangle$
  - Column 9: combined uncertainty on $\langle HWS \rangle$ (k=1).

Table 4. Analysis of uncertainty components for y_m and $Ref_{eq\ RWS}$ (ZDM351)

1	2	3	4	5	6	7	8	9	10
Bin	Lower RWS	Upper RWS	U HWS to ref	U tilt to ref	U Wdrel to ref	Uc ref	U ym ref	U ym gain	Uc ym
-	[m/s]	[m/s]	[m/s]	[m/s]	[m/s]	[m/s]	[m/s]	[m/s]	[m/s]
…	…	…	…	…	…	…	…	…	…
10	4,75	5,25	0,0596	0,0001	0,0143	0,0613	0,0616	0,0056	0,0618
11	5,25	5,75	0,0635	0,0001	0,0146	0,0651	0,0654	0,0062	0,0657
12	5,75	6,25	0,0669	0,0002	0,0172	0,0690	0,0694	0,0067	0,0697
…	…	…	…	…	…	…	…	…	…
25	12,25	12,75	0,1175	0,0003	0,0340	0,1223	0,1230	0,0139	0,1237
26	12,75	13,25	0,1214	0,0003	0,0371	0,1269	0,1276	0,0145	0,1284
…	…	…	…	…	…	…	…	…	…

Table 5. Analysis of uncertainty components for $\langle HWS \rangle_{vec}$ (ZDM351)

1	2	3	4	5	6	7	8	9
Bin	Lower RWS	Upper RWS	U cal tot	U ope tot	U mast	U pos	U inc	Uc HWS
-	[m/s]	[m/s]	[m/s]	[m/s]	[m/s]	[m/s]	[m/s]	[m/s]
…	…	…	…	…	…	…	…	…
10	4,75	5,25	0,0399	0,0399	0,0269	0,0124	0,0056	0,0639
11	5,25	5,75	0,0421	0,0412	0,0294	0,0135	0,0061	0,0674
12	5,75	6,25	0,0449	0,0427	0,0323	0,0148	0,0067	0,0717
…	…	…	…	…	…	…	…	…
25	12,25	12,75	0,0810	0,0606	0,0666	0,0306	0,0138	0,1255
26	12,75	13,25	0,0844	0,0622	0,0697	0,0321	0,0145	0,1306
…	…	…	…	…	…	…	…	…

Figure 23 illustrates the uncertainty assessment procedure in the form of a "tree" structure. The analysis of the contributions[8] of each component to the next level of uncertainties shows that:

- The reference quantitiy value uncertainty $Ref_{eq\ RWS}$ accounts for 99% of the combined uncertainty on y_m;
- ~90% of $u_{c,Ref_{eq\ RWS}}$ is related to the HWS uncertainty;
- ~94% of the HWS uncertainty is due to the calibration, operational and mast uncertainties, and thus the calibration process uncertainty accounts for the remaining 6% with u_{inc} and u_{pos}.

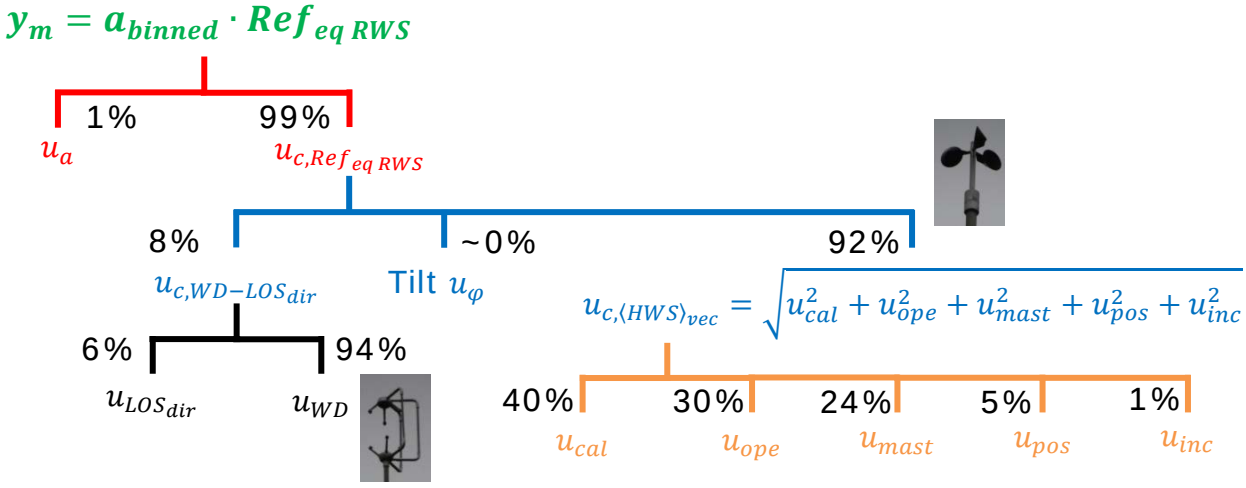

Figure 23. The "tree" structure of the uncertainty assessment methodology

[8] The contributions (in %) provided in Figure 23 correspond to the calibration results of ZDM351 with a 2°-wide azimuth sector for averaging the LOS velocity.

4.2.4 Summary of calibration uncertainty results

Table 6 provides bin-wise expanded uncertainties for each LOS and with a coverage factor $k = 2$ ($\equiv 95\%$ confidence interval assuming normal distribution of uncertainties). In each bin, the expanded uncertainties are expressed in $m.s^{-1}$ and $\%$ of the bin center.

Table 6. Summary of calibration uncertainty results – bin-wise expanded uncertainties (ZDM351)

Bin	RWS bin center [m/s]	ZDM351 '2° azimuth'	
		m/s	*%*
6	[2.75; 3.25[	0,096	3,20%
7	[3.25; 3.75[	0,102	2,91%
8	[3.75; 4.25[	0,110	2,75%
9	[4.25; 4.75[	0,116	2,58%
10	[4.75; 5.25[	0,124	2,48%
11	[5.25; 5.75[	0,131	2,38%
12	[5.75; 6.25[	0,139	2,32%
13	[6.25; 6.75[	0,148	2,28%
14	[6.75; 7.25[	0,156	2,23%
15	[7.25; 7.75[	0,165	2,20%
16	[7.75; 8.25[	0,172	2,15%
17	[8.25; 8.75[	0,179	2,11%
18	[8.75; 9.25[	0,188	2,09%
19	[9.25; 9.75[	0,197	2,07%
20	[9.75; 10.25[	0,204	2,04%
21	[10.25; 10.75[	0,213	2,03%
22	[10.75; 11.25[	0,222	2,02%
23	[11.25; 11.75[	0,230	2,00%
24	[12.75; 12.25[	0,238	1,98%
25	[12.25; 12.75[	0,247	1,98%
26	[12.75; 13.25[	0,257	1,98%
27	[13.25; 13.75[	0,266	1,97%
28	[13.75; 14.25[	0,274	1,96%
29	[14.25; 14.75[	0,276	1,90%
30	[14.75; 15.25[	0,282	1,88%
31	[15.25; 15.75[	0,294	1,90%
32	[15.75; 16.25[	0,302	1,89%

As the calibration is performed in uncontrolled conditions, the criteria on the minimum number of points per bin may not be met in certain bins. In those bins (shown in red), no uncertainties are obtained experimentally and the uncertainty values may be extrapolated using the linear regressions previously obtained (see e.g. Figure 21 or Table 10). For the ZDM351 lidar, the extrapolation formula is:

$$U_{ext,0} = 0.01617 \cdot RWS\ bin\ center + 0.04368 \qquad [m.s^{-1}]$$

4.3 Deriving uncertainties of reconstructed parameters: example HWS from a "4-beam" nacelle lidar

In this paragraph, the principles of how to combine the uncertainties from different LOS are exemplified through an arbitrary reconstruction algorithm. The reconstructed parameter example is the horizontal wind speed derived from a "4-beam" nacelle lidar, i.e. four azimuth sectors arranged in a square pattern are used and the LOS velocity is averaged in each sector. The "4 beams" are here denoted as LOS_{TL}, LOS_{TR}, LOS_{BL}, LOS_{BR} respectively corresponding to the top left, top right, bottom left, bottom right positions (Figure 24).

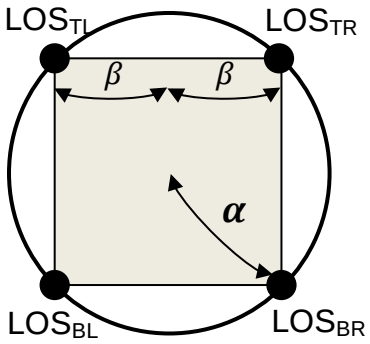

Figure 24. Beam positions of simulated 4-beam nacelle lidar from the ZDM

NB: using more complex reconstruction techniques, the ZDM lidar can be used e.g. as a 48-beam lidar and a wind model fitted to the averaged LOS velocity measurements.

The methodology to obtain the uncertainty of the reconstructed parameter is based on the GUM ([6]). The degree of correlation between the various calibration uncertainty components (see 4.1) is discussed, and the impact on the total uncertainty on the reconstructed parameter investigated.

In terms of uncertainties, when considering correlated or uncorrelated uncertainties, the question to answer is: when the RWS along one beam i is evaluated with an error $+a$ due to one uncertainty source (e.g. the cup calibration uncertainty), does beam j makes the same error ($R_{ij} = 1$), an error $-a$ ($R_{ij} = -1$) or a random error ($R_{ij} = 0$). The authors recommend reading §5.2 in [6], which details the theory of correlated uncertainties and provides metrological examples

4.3.1 Horizontal wind speed reconstruction

An algorithm to reconstruct the horizontal wind vector via its longitudinal and transverse components denoted U and V respectively, is described. The algorithm uses the top (LOS_{TL} and LOS_{TR}) and bottom (LOS_{BL} and LOS_{BR}) pairs of beams. Assuming horizontal flow homogeneity, we first express U_{top} and V_{top}:

$$\begin{cases} U_{top} = \dfrac{(V_{rTL} + V_{rTR})}{2cos\beta_h cos\beta_v} \\ V_{top} = \dfrac{(V_{rTL} - V_{rTR})}{2sin\beta_h cos\beta_v} \end{cases}$$

Where V_{rX} is the 10-minute averaged of the RWS along LOS X, β_h and β_v are the horizontal and vertical half-opening angles respectively.

Note: in the case of the 4-beam lidar simulated from ZDM, $\beta_h = \beta_v = \beta \approx \text{atan}\left(\tan(\alpha_{th})/\sqrt{2}\right) = 10.71°$.

Similarly for the bottom pair, LOS_{TL} is substituted by LOS_{BL} and LOS_{TR} by LOS_{BR} (see Figure 24). We obtain:

$$\begin{cases} U_{bot} = \dfrac{(V_{rBL} + V_{rBR})}{2cos\beta_h cos\beta_v} \\ V_{bot} = \dfrac{(V_{rBL} - V_{rBR})}{2sin\beta_h cos\beta_v} \end{cases}$$

Assuming linear vertical profiles of U and V, the wind vector components at hub height are:

$$\begin{cases} U_{hub} = \dfrac{U_{top} + U_{bot}}{2} = \dfrac{V_{rTL} + V_{rTR} + V_{rBL} + V_{rBR}}{4cos\beta_h cos\beta_v} \\ V_{hub} = \dfrac{V_{top} + V_{bot}}{2} = \dfrac{(V_{rTL} - V_{rTR}) + (V_{rBL} - V_{rBR})}{4sin\beta_h cos\beta_v} \end{cases}$$

The horizontal speed at hub height is simply:

$$S_{hub} = \sqrt{U_{hub}^2 + V_{hub}^2}$$

4.3.2 Method to combine radial wind speed uncertainties

For the uncertainties, the simplest model is to take the case of $V_{hub} = 0$, i.e. no yaw misalignment. It can be shown that for small and realistic values of yaw error, the uncertainties of the U component dominate (since this is by far the largest component numerically) but as yaw error increases, the V uncertainties begin to become significant (because of the term $\sin\beta_h \ll 1$ in the denominator).

For zero yaw error, the horizontal speed is simply the U component:

$$S_{hub} = \frac{V_{rTL} + V_{rTR} + V_{rBL} + V_{rBR}}{4cos\beta_h cos\beta_v}$$

The uncertainty of the horizontal speed $U(S_{hub})$ will depend critically on the correlation between the uncertainties of the 4 radial speeds. Three different cases are thus investigated hereafter:

- No correlation
- Full correlation
- Partial correlation

4.3.2.1 Case 1: no correlation

For completely uncorrelated uncertainties, and neglecting the contribution of the opening angles to the uncertainty, we will simply have:

$$U(S_{hub}) = \frac{1}{4cos\beta_h cos\beta_v}\sqrt{U(V_{rBL})^2 + U(V_{rTR})^2 + U(V_{rBL})^2 + U(V_{rBR})^2}$$

If all 4 radial speed uncertainties are equal and given by $U(V_r)$, this simplifies to:

$$U(S_{hub}) = \frac{U(V_r)}{2cos\beta_h cos\beta_v}$$

With $\beta_h = \beta_v = 10.71°$, we obtain: $U(S_{hub}) \approx 52\% \cdot U(V_r)$.

4.3.2.2 Case 2: full correlation

At the other extreme, if all the radial speed uncertainties are fully correlated, the RWS uncertainties must be added arithmetically and we obtain:

$$U(S_{hub}) = \frac{U(V_{rBL}) + U(V_{rTR}) + U(V_{rBL}) + U(V_{rBR})}{4cos\beta_h cos\beta_v}$$

If all 4 radial speed uncertainties are equal to $U(V_r)$, then:

$$U(S_{hub}) = \frac{U(V_r)}{cos\beta_h cos\beta_v}$$

which is twice as large as for the uncorrelated case. This shows how important it is to consider the correlation between each component of the different beams' RWS uncertainty.

4.3.2.3 Case 3: partial correlation

In the general case, the RWS uncertainties $U(V_{ri})$ are partially correlated. The cross-correlation matrix R (of size 4x4) provides the degree of correlation between pairs of beams:

$$R = \begin{bmatrix} 1 & r_{12} & r_{13} & r_{14} \\ r_{12} & 1 & r_{23} & r_{24} \\ r_{13} & r_{23} & 1 & r_{34} \\ r_{14} & r_{24} & r_{34} & 1 \end{bmatrix}$$

The non-unit cross-correlation coefficients may have different for different uncertainty components. Simplifying by considering the correlation between RWSs uncertainties instead of the correlation between individual uncertainty components, the uncertainty on the reconstructed horizontal wind speed is in the partial correlation case:

$$U(S_{hub}) = \frac{1}{4cos\beta_h cos\beta_v} \sqrt{\sum_{i=1}^{4} U^2(V_{ri}) + 2\sum_{i=1}^{4}\sum_{j=i+1}^{4} R_{ij} U(V_{ri}) U(V_{rj})}$$

4.3.3 Correlation between RWS uncertainties

In this paragraph, we discuss which case of the three previously mentioned should be used to combine the RWS uncertainties. For the sake of simplicity, we here assume uncertainty components to be either fully correlated or fully uncorrelated. In the case of the ZDM lidar, the same beam parcours the circular scan trajectory. Thus, all the uncertainty components of each of the four LOSs defined previously defined (see Figure 24) are fully correlated, i.e. the calibration of the bottom part of the scanning pattern is considered valid for all other azimuth sectors. Consequently, one might choose the 2nd case, i.e. full correlation.

Note: this discussion suggests that reducing the RWS measurement uncertainties of lidars could be achieved by using different wind speed reference instruments calibrated in different wind tunnels and by calibrating each LOS separately (instead of once) at a different site. This highlights the weaknesses of the methodology to assess wind speed uncertainty from cup anemometers that is provided by standards.

Second, the distribution of calibration results observed between different lidars' beams is much smaller than would be the case if the uncertainties between LOSs (both with the same or different lidar units) were uncorrelated. If the RWS uncertainties were truly uncorrelated, one would expect the width of the distribution of the calibration results to be of a similar size as the RWS uncertainties. This is not the case: the gain values of the forced linear regressions are within a 0.5% range. The explanation can be that either the RWS uncertainties are overestimated (probably due to the cup anemometer) or the narrow distribution is a result of seeing the same (unknown) error repeatedly (correlated uncertainty).

Finally, the fully correlated case is the most conservative of the three. For all those reasons, it is suggested to use case 2 (4.3.2.2) to combine uncertainties of reconstructed parameters.

In practice, once measuring from the nacelle of the wind turbines, the lidar will not measure the same values of V_r. since the bottom LOSs will sense winds at a lower height than the top LOSs. And, for each 10min a non-zero yaw misalignement is expected. Using fully correlated uncertainties, we would obtain:

$$\begin{cases} U_{hub} = \dfrac{U_{top} + U_{bot}}{2} = \dfrac{V_{rTL} + V_{rTR} + V_{rBL} + V_{rBR}}{4cos\beta_h cos\beta_v} \\ V_{hub} = \dfrac{V_{top} + V_{bot}}{2} = \dfrac{(V_{rTL} - V_{rTR}) + (V_{rBL} - V_{rBR})}{4sin\beta_h cos\beta_v} \end{cases}$$

As the transverse component V_{hub} should be lower than U_{hub}, a lower uncertainty is also obtained due to the minus signs.

Conclusion

In this document, the calibration of a ZephIR Dual-Mode lidar is reported in details, both from the methods and results point of views. The 'white box' calibration methodology was employed. The calibration results proved to be consistent, with a high level of agreement between the measured radial wind speed and reference quantity values. Sensitivity of the lidar's measurements to environmental parameters was investigated and showed that most environmental parameters do not have a significant impact on the lidar's measurement accuracy. Radial wind speed measurement uncertainties were assessed and the methods to do so is provided. An arbitrary example of reconstruction algorithm was finally used to exemplify how to combine the radial wind speed uncertainties and estimate uncertainties on wind parameters.

Traceable measurements to national standards can thus be obtained from the ZephIR Dual-Mode (unit 351) lidar using the information contained in this report.

Annexes

Annex A. Calibration of the tilt inclination angle: measurement uncertainties

Using the notation in 2.4, the measurement model is:

$$\varphi_{mod} = \frac{\varphi_{meas} - offset}{gain}$$

Where:

$$\begin{cases} gain = 0.9901\ [°/°] \\ offset = 0.3856° = 6.73 \cdot 10^{-3} rad \end{cases}$$

This measurement model corresponds to the following correction of the lidar indicated tilt (φ_{BE} is the best estimate of the tilt angle using the lidar indication):

$$\varphi_{BE} = gain \cdot \varphi_{indicated} + offset$$

Applying the GUM methodology to the measurement model, the combined uncertainty φ_{mod} is obtained (coverage factor $k = 1$):

$$u_{c,\varphi_{mod}} = \sqrt{\frac{\left(u_{\varphi_{meas}}^2 + u_{offset}^2\right)}{gain^2} + (\varphi_{meas} - offset)^2 \cdot u_{gain}^2} \qquad \text{(eq. 6)}$$

The uncertainties on the gain and offset are taken as the half-with of the 68% (equivalent to $k = 1$) confidence interval obtained using the unforced linear regression's statistics:

$$\begin{cases} u_{gain} = 0.002166\ [°/°] \\ u_{offset} = 0.006259° = 1.09 \cdot 10^{-4} rad \end{cases}$$

The uncertainty on the reference measurement angle is obtained by applying the GUM methodology to the measurements conducted in 2.4.1. After simplifications, the combined uncertainty is:

$$u_{c,\varphi_{meas}} = u_{c,\varphi_{beam}} = \text{atan}\left(\frac{u_{\Delta Z}}{D_{ref}}\right)$$

Conservative estimates of the uncertainties of the beam detection and total station measurements are: $10\ mm$ (beam position). Thus $u_{\Delta Z} = 10mm \cdot \sqrt{2}$. At the distance $D_{ref} \approx 10m$, the combined uncertainty on φ_{meas} is $u_{\varphi_{meas}} = 0.081°$.

Since $gain \approx 1$, $u_{offset}^2 \ll u_{\varphi_{meas}}^2$ and $(\varphi_{meas} - offset)^2 \cdot u_{gain}^2 \ll u_{\varphi_{meas}}^2$, (eq. 6) is approximated and simplified to:

$$u_{c,\varphi_{mod}} = u_{\varphi_{ref}}$$

Finally, the expanded uncertainty with a coverage factor $k = 2$ is: $\boldsymbol{U_{\varphi_{BE}} = k \cdot u_{c,\varphi_{mod}} = 0.16°}$.

Annex B. Calibration certificate of cup anemometer

Deutsche WindGuard
Wind Tunnel Services GmbH, Varel

Deutsche WindGuard

1108/2722

akkreditiert durch die / *accredited by the*

Deutsche Akkreditierungsstelle GmbH

DAkkS Deutsche Akkreditierungsstelle D-K-15140-01-00

als Kalibrierlaboratorium im / *as calibration laboratory in the*

Deutschen Kalibrierdienst DKD

	1323249
	D-K-15140-01-00
Calibration mark	10/2013

Kalibrierschein
Calibration certificate

Gegenstand *Object*	Cup Anemometer
Hersteller *Manufacturer*	Thies Clima D-37083 Göttingen
Typ *Type*	4.3351.10.000
Fabrikat/Serien-Nr. *Serial number*	11116763 2722
Auftraggeber *Customer*	Risoe DTU DK-4000 Roskilde
Auftragsnummer *Order No.*	VT131006
Anzahl der Seiten des Kalibrierscheines *Number of pages of the certificate*	3
Datum der Kalibrierung *Date of calibration*	24.10.2013

Dieser Kalibrierschein dokumentiert die Rückführung auf nationale Normale zur Darstellung der Einheiten in Übereinstimmung mit dem Internationalen Einheitensystem (SI).
Die DAkkS ist Unterzeichner der multilateralen Übereinkommen der European co-operation for Accreditation (EA) und der International Laboratory Accreditation Cooperation (ILAC) zur gegenseitigen Anerkennung der Kalibrierscheine.
Für die Einhaltung einer angemessenen Frist zur Wiederholung der Kalibrierung ist der Benutzer verantwortlich.

This calibration certificate documents the traceability to national standards, which realize the units of measurement according to the International System of Units (SI).
The DAkkS is signatory to the multilateral agreements of the European co-operation for Accreditation (EA) and of the International Laboratory Accreditation Cooperation (ILAC) for the mutual recognition of calibration certificates.
The user is obliged to have the object recalibrated at appropriate intervals.

Datum *Date*	Leiter des Kalibrierlaboratoriums *Head of the calibration laboratory*	Bearbeiter *Person in charge*
24.10.2013	Dipl. Phys. D. Westermann	Technikerin Bilke Engelbrecht

Seite 2
Page

1323249
D-K-15140-01-00
10/2013

Kalibriergegenstand *Object*	Cup Anemometer		
Kalibrierverfahren *Calibration procedure*	IEC 61400-12-1 – Power performance measurements of electricity producing wind turbines – 2005-12 ISO 3966 – Measurement of fluid in closed conduits – 2008-07		
Ort der Kalibrierung *Place of calibration*	Windtunnel of Deutsche WindGuard, Varel		
Messbedingungen *Test Conditions*	wind tunnel area [1]	10000 cm²	
	anemometer frontal area [2]	230 cm²	
	diameter of mounting pipe [3]	34 mm	
	blockage ratio [4]	0.023 [-]	
	blockage correction [5]	1.000 [-]	
Umgebungsbedingungen *Test conditions*	air temperature	22.9 °C	± 0.1 K
	air pressure	1017.5 hPa	± 0.3 hPa
	relative air humidity	53.7 %	± 2.0 %
Akkreditierung *Accreditation*	01/2013		
Anmerkungen *Remarks*	Calibration after refurbishment		
Auswertesoftware *Software version*	7.58		

[1] Querschnittsfläche der Auslassdüse des Windkanals
[2] Vereinfachte Querschnittsfläche (Schattenwurf) des Prüflings inkl. Montagerohr
[3] Durchmesser des Montagerohrs
[4] Verhältnis von 2) zu 1)
[5] Korrekturfaktor durch die Verdrängung der Strömung durch den Prüfling
Anmerkung: Aufgrund der speziellen Konstruktion der Messstrecke ist keine Korrektur nötig.
Remark: Due to the special construction of the test section no blockage correction is necessary

Dieser Kalibrierschein wurde elektronisch erzeugt
This calibration certificate has been generated electronically

Seite 3
Page

1323249
D-K-15140-01-00
10/2013

Kalibrierergebnis:
Result:

File:	1323249	
Test Item (1/s)	Tunnel Speed (m/s)	Uncertainty (k=2) (m/s)
82.449	4.018	0.050
124.924	5.986	0.050
169.001	8.019	0.050
212.344	9.996	0.051
256.175	12.024	0.051
298.122	13.974	0.051
342.208	15.956	0.051
321.984	15.015	0.051
277.958	13.013	0.051
233.498	10.981	0.051
190.816	9.023	0.051
147.893	7.033	0.050
103.351	4.980	0.050

Angegeben ist die erweiterte Messunsicherheit, die sich aus der Standardmessunsicherheit durch Multiplikation mit dem Erweiterungsfaktor k=2 ergibt. Sie wurde gemäß DAkkS-DKD-3 ermittelt. Der Wert der Messgröße liegt mit einer Wahrscheinlichkeit von 95 % im zugeordneten Wertintervall.

Die Deutsche Akkreditierungsstelle GmbH ist Unterzeichnerin der multilateralen Übereinkommen der European co-operation for Accreditation (EA) und der International Laboratory Accreditation Cooperation (ILAC) zur gegenseitigen Anerkennung der Kalibrierscheine. Die weiteren Unterzeichner innerhalb und außerhalb Europas sind den Internetseiten von EA (www.european-accreditation.org) und ILAC (www.ilac.org) zu entnehmen.

The expanded uncertainty assigned to the measurement results is obtained by multiplying the standard uncertainty by the coverage factor k = 2. It has been determined in accordance with DAkkS-DKD-3. The value of the measurand lies within the assigned range of values with a probability of 95%.

The DAkkS is signatory to the multilateral agree-ments of the European co-operation for Accredita-tion (EA) and of the International Laboratory Accreditation Cooperation (ILAC) for the mutual recognition of calibration certificates.

Anhang
Annex

1323249

1 Detailed Calibration Results

DKD calibration no.	1323249
Body no.	11116763
Cup no.	2722
Date	24.10.2013
Air temperature	22.9 °C
Air pressure	1017.5 hPa
Humidity	53.7 %

Linear regression analysis

Slope	0.04597 (m/s)/(1/s) ±0.00005 (m/s)/(1/s)
Offset	0.2388 m/s ±0.012 m/s
St.err(Y)	0.013 m/s
Correlation coefficient	0.999993

Remarks no

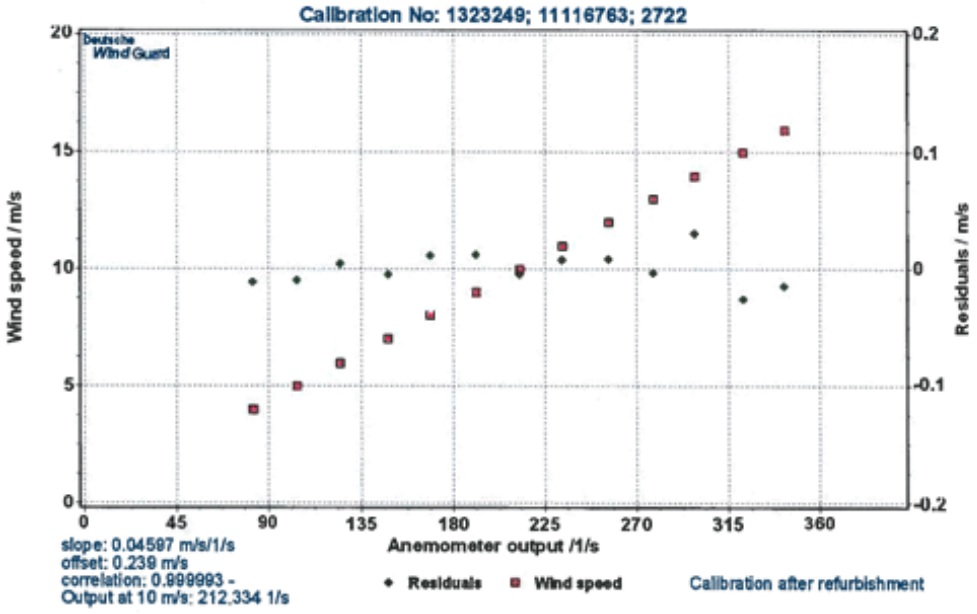

Deutsche WindGuard Wind Tunnel Services is accredited by MEASNET and by the Deutsche Akkreditierungsdienst – DAkkS (German Accreditation Service). Registration: D-K-15140-01-00

Anhang
Annex

1323249

2 Instrumentation

Pos.	Sensor	Manufa.	Type	Range
1	Pitot static tube	Airflow	NPL 8 mm	-
2	Pitot static tube	Airflow	NPL 8 mm	-
3	Pitot static tube	Airflow	NPL 8 mm	-
4	Pitot static tube	Airflow	NPL 8 mm	-
5	Pressure transducer	Setra	C 239	250 Pa
6	Pressure transducer	Setra	C 239	250 Pa
7	Pressure transducer	Setra	C 239	250 Pa
8	Pressure transducer	Setra	C 239	250 Pa
9	El. Barometer	Vaisala	3.11.57.10.000	800hPa -1200 hPa
10	El. Thermometer	Galltec	KPK 1/6-ME	10° C - 40° C
11	El. Humidity sensor	Galltec	KPK 1/6-ME	0-100 %
12	Wind tunnel control	-	-	-
13	CAN-BUS / PC	esd	24 x 16 bit	

Table 1 Description of the data acquisition system
Remark: Last Re-accreditation see page 2

3 Photo of the calibration set-up

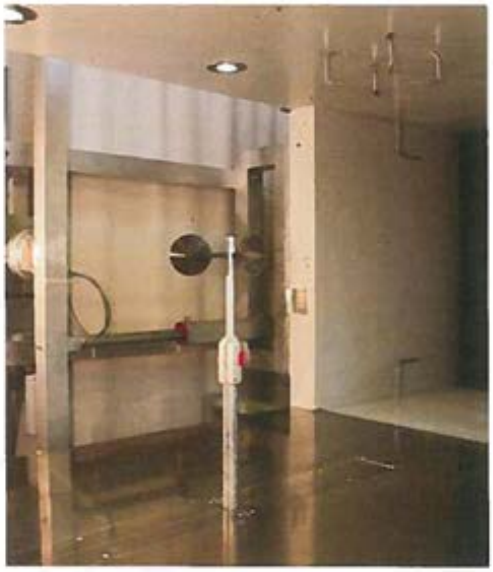

Calibration set-up of the anemometer calibration in the wind tunnel of Deutsche WindGuard, Varel. The anemometer and orientation shown may differ from the calibrated one. Remark: The proportion of the set-up is not true to scale due to imaging geometry.

4 Deviation to IEC procedure

The calibration procedure is in all aspects in accordance with the IEC 61400-12-1 Procedure

5 References

[1] D. Westermann, 2009 – Verfahrensanweisung DKD-Kalibrierung von Windgeschwindigkeitssensoren
[2] IEC 61400-12-1 12/2005 – Power performance measurements of electricity producing wind turbines
[3] ISO 3966 2008 – Measurement of fluid flow in closed conduits

Annex C. Calibration certificate of sonic anemometer, for wind direction, at 0° inflow

Deutsche WindGuard
Wind Tunnel Services GmbH, Varel

Deutsche WindGuard

7820/0845

akkreditiert durch die / *accredited by the*

Deutsche Akkreditierungsstelle GmbH

DAkkS Deutsche Akkreditierungsstelle D-K-15140-01-00

als Kalibrierlaboratorium im / *as calibration laboratory in the*

Deutschen Kalibrierdienst DKD

1322749	
D-K-15140-01-00	
Calibration mark	09/2013

Kalibrierschein
Calibration certificate

Gegenstand *Object*	Sonic Anemometer	
Hersteller *Manufacturer*	Gill Instruments UK-Hampshire S041 9EG	
Typ *Type*	1210R3	
Fabrikat/Serien-Nr. *Serial number*	000078	
Auftraggeber *Customer*	Risoe DTU DK-4000 Roskilde	
Auftragsnummer *Order No.*		VT130930
Anzahl der Seiten des Kalibrierscheines *Number of pages of the certificate*		5
Datum der Kalibrierung *Date of calibration*		13.09.2012

Dieser Kalibrierschein dokumentiert die Rückführung auf nationale Normale zur Darstellung der Einheiten in Übereinstimmung mit dem Internationalen Einheitensystem (SI).
Die DAkkS ist Unterzeichner der multilateralen Übereinkommen der European co-operation for Accreditation (EA) und der International Laboratory Accreditation Cooperation (ILAC) zur gegenseitigen Anerkennung der Kalibrierscheine.
Für die Einhaltung einer angemessenen Frist zur Wiederholung der Kalibrierung ist der Benutzer verantwortlich.
This calibration certificate documents the traceability to national standards, which realize the units of measurement according to the International System of Units (SI).
The DAkkS is signatory to the multilateral agreements of the European co-operation for Accreditation (EA) and of the International Laboratory Accreditation Cooperation (ILAC) for the mutual recognition of calibration certificates.
The user is obliged to have the object recalibrated at appropriate intervals.

Datum *Date*	Leiter des Kalibrierlaboratoriums *Head of the calibration laboratory*	Bearbeiter *Person in charge*
16.09.2012	Dipl. Phys. D. Westermann	Dipl.-Ing. (FH) Catharina Herold

Seite 2 *Page*	1322749 D-K-15140-01-00 09/2013

Kalibriergegenstand
Object
Sonic Anemometer

Ort der Kalibrierung
Place of calibration
Windtunnel of Deutsche WindGuard, Varel

Kalibrierverfahren
Calibration procedure
ASTM 5366-96 Standard Test Method of Measuring the Dynamic Performance of Wind Vanes - 2002
Deutsche WindGuard Verfahrensanweisung Kalibrierung von Windrichtungssensoren

Die messtechnische Bestimmung der angezeigten Windrichtung eines Windrichtungssensors zur Strömungsrichtung im Windkanal erfolgt mit Hilfe einer Dreheinrichtung unterhalb der Messstrecke des Windkanals. Während der Messung wird der Windrichtungssensor kontinuierlich von 0 Grad bis 40 Grad und zurück nach 320 Grad bei konstanter Strömungsgeschwindigkeit gedreht. Die Mittelwertbildung erfolgt in Klassen (Klassenbreite siehe Seite 3).

The measurement of the indicated direction of a wind vane to statically yawed air flow is done with the help of an automatic yaw device installed below the wind tunnel test section. During the measurements, the wind vane is yawed continuously from 0 to 40 degrees and back to 320 degree at constant flow speed. The data are bin-averaged in classes (see page 3).

Umgebungsbedingungen:
Test conditions

air temperature:	24.5 °C
air pressure:	1017.4 hPa
relative air humidity:	56.4 %

Kommentar:
Comment
Tilt orientation: 0 deg

Akkreditierung:
Accreditation
01/2013

Dieser Kalibrierschein wurde elektronisch erzeugt
This calibration certificate has been generated electronically

Seite 3
Page

1322749
D-K-15140-01-00
09/2013

Kalibrierergebnis:
Result:

File:	1322749					
Bin	Flow Dir	dir	v_hor	v_ver	Unc	Flow speed
-	deg	deg	m/s	m/s	deg	m/s
1	0.99	0.854	7.940	-0.103	0.8	8.139
2	1.98	1.939	7.950	-0.097	0.8	8.138
3	3.06	2.909	7.944	-0.102	0.8	8.139
4	4.05	4.023	7.952	-0.101	0.8	8.137
5	5.02	5.265	7.950	-0.101	0.8	8.136
6	6.03	6.814	7.963	-0.092	0.8	8.139
7	7.00	7.000	7.956	-0.083	0.8	8.129
8	8.00	7.918	7.964	-0.089	0.8	8.141
9	9.02	8.979	7.969	-0.089	0.8	8.137
10	9.96	9.977	7.965	-0.088	0.8	8.139
11	10.98	11.023	7.954	-0.093	0.8	8.141
12	11.97	12.333	7.948	-0.094	0.8	8.143
13	12.98	13.771	7.960	-0.100	0.8	8.135
14	14.03	14.000	7.965	-0.103	0.8	8.139
15	15.01	15.163	7.959	-0.106	0.8	8.133
16	16.02	16.085	7.964	-0.108	0.8	8.136
17	17.05	17.292	7.969	-0.113	0.8	8.144
18	18.01	18.023	7.968	-0.113	0.8	8.140
19	18.98	19.313	7.972	-0.115	0.8	8.140
20	20.01	20.625	7.965	-0.114	0.8	8.138
21	20.99	21.026	7.971	-0.117	0.8	8.144
22	21.98	22.481	7.977	-0.117	0.8	8.140
23	23.06	23.041	7.982	-0.121	0.8	8.139
24	24.02	24.717	7.972	-0.124	0.8	8.142
25	25.00	25.851	7.984	-0.122	0.8	8.138
26	26.12	26.045	7.969	-0.126	0.8	8.140
27	27.01	27.098	7.965	-0.125	0.8	8.137
28	27.95	27.980	7.966	-0.130	0.8	8.141
29	29.00	29.540	7.967	-0.124	0.8	8.137
30	29.88	29.951	7.961	-0.125	0.8	8.139
31	30.94	31.306	7.979	-0.123	0.8	8.144
32	32.03	32.490	7.978	-0.123	0.8	8.141
33	33.04	33.279	7.970	-0.117	0.8	8.136
34	34.04	34.447	7.989	-0.110	0.8	8.137
35	35.03	35.410	7.994	-0.115	0.8	8.141
36	36.01	37.000	8.000	-0.112	0.8	8.141
37	37.01	37.279	7.998	-0.111	0.8	8.142
38	37.98	39.071	7.990	-0.105	0.8	8.142
39	38.94	39.795	8.005	-0.102	0.8	8.139
40	39.95	40.463	8.002	-0.096	0.8	8.140

Seite 4
Page

1322749
D-K-15140-01-00
09/2013

File:	1322749					
Bin	Flow Dir	dir	v_hor	v_ver	Unc	Flow speed
-	deg	deg	m/s	m/s	deg	m/s
41	319.96	319.136	7.996	0.010	0.8	8.140
42	320.93	321.118	8.009	0.006	0.8	8.141
43	321.96	321.933	8.006	0.008	0.8	8.141
44	322.96	322.000	7.993	-0.001	0.8	8.141
45	324.00	322.754	7.985	-0.002	0.8	8.142
46	325.07	324.135	7.996	-0.003	0.8	8.132
47	326.07	325.531	7.998	-0.005	0.8	8.133
48	327.00	326.698	8.004	-0.010	0.8	8.138
49	328.04	328.509	8.002	-0.019	0.8	8.141
50	329.01	328.755	7.991	-0.021	0.8	8.136
51	329.98	329.460	7.992	-0.026	0.8	8.136
52	330.98	330.811	8.001	-0.025	0.8	8.139
53	331.99	331.818	7.967	-0.031	0.8	8.133
54	332.98	332.966	7.966	-0.031	0.8	8.137
55	334.08	333.778	7.985	-0.031	0.8	8.134
56	335.07	335.043	7.987	-0.026	0.8	8.140
57	336.01	335.940	7.984	-0.028	0.8	8.137
58	337.09	336.556	7.986	-0.032	0.8	8.141
59	337.98	337.778	7.985	-0.034	0.8	8.138
60	338.95	338.824	7.985	-0.039	0.8	8.144
61	339.99	340.400	7.981	-0.041	0.8	8.142
62	340.96	340.896	7.970	-0.045	0.8	8.138
63	342.02	341.021	7.966	-0.054	0.8	8.140
64	342.99	342.654	7.963	-0.059	0.8	8.138
65	344.00	344.122	7.963	-0.057	0.8	8.141
66	345.02	345.000	7.970	-0.059	0.8	8.143
67	345.98	345.619	7.954	-0.061	0.8	8.137
68	347.01	347.353	7.965	-0.070	0.8	8.141
69	348.03	348.143	7.971	-0.071	0.8	8.140
70	348.97	349.467	7.968	-0.078	0.8	8.143
71	349.94	350.078	7.945	-0.085	0.8	8.143
72	350.93	351.400	7.958	-0.091	0.8	8.144
73	351.93	352.021	7.939	-0.080	0.8	8.138
74	352.98	352.782	7.943	-0.079	0.8	8.139
75	354.08	354.804	7.945	-0.085	0.8	8.136
76	355.01	355.000	7.950	-0.083	0.8	8.139
77	355.96	356.083	7.964	-0.089	0.8	8.144
78	357.03	357.000	7.962	-0.097	0.8	8.141

Angegeben ist die erweiterte Messunsicherheit, die sich aus der Standardmessunsicherheit durch Multiplikation mit dem Erweiterungsfaktor k=2 ergibt. Sie wurde gemäß DAkkS-DKD-3 ermittelt. Der Wert der Messgröße liegt mit einer Wahrscheinlichkeit von 95 % im zugeordneten Wertintervall.

Die Deutsche Akkreditierungsstelle GmbH ist Unterzeichnerin der multilateralen Übereinkommen der European co-operation for Accreditation (EA) und der International Laboratory Accreditation Cooperation (ILAC) zur gegenseitigen Anerkennung der Kalibrierscheine. Die weiteren Unterzeichner innerhalb und außerhalb Europas sind den Internetseiten von EA (www.european-accreditation.org) und ILAC (www.ilac.org) zu entnehmen.

The expanded uncertainty assigned to the measurement results is obtained by multiplying the standard uncertainty by the coverage factor k = 2. It has been determined in accordance with DAkkS-DKD-3. The value of the measurand lies within the assigned range of values with a probability of 95%.

The DAkkS is signatory to the multilateral agree-ments of the European co-operation for Accredita-tion (EA) and of the International Laboratory Accreditation Cooperation (ILAC) for the mutual recognition of calibration certificates

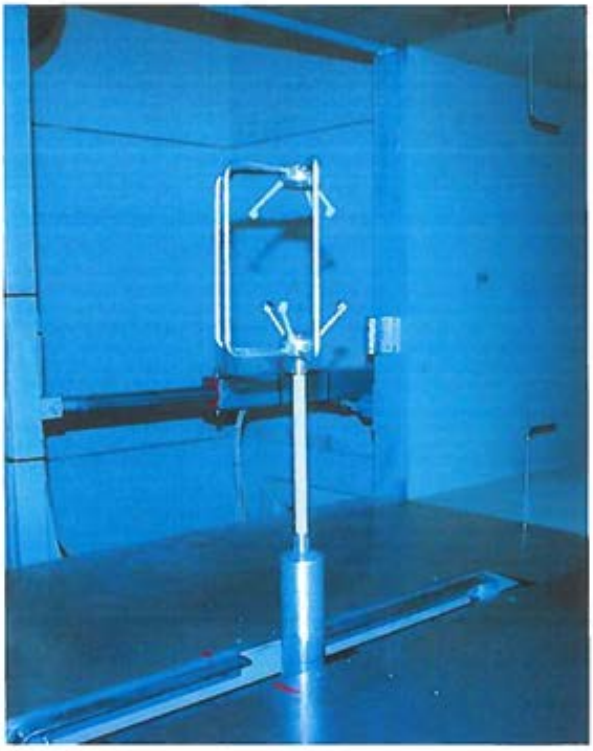

Image 1: Calibration set-up of flow direction test in the wind tunnel of Deutsche WindGuard, Varel. The sensor shown may differ from the calibrated one. Remark: The proportion of the set-up is not true to scale due to imaging geometry.

Annex D. Fine tilt adjustment system for ZDM lidar

To point the beam of the ZDM lidar at the desired height (the one of the two small masts), a fine-tuning tilting system was attached to the rear leg of the ZDM lidar (Figure 25). The fine-tuning system has been designed by DTU Wind Energy technicians (L. Christensen).

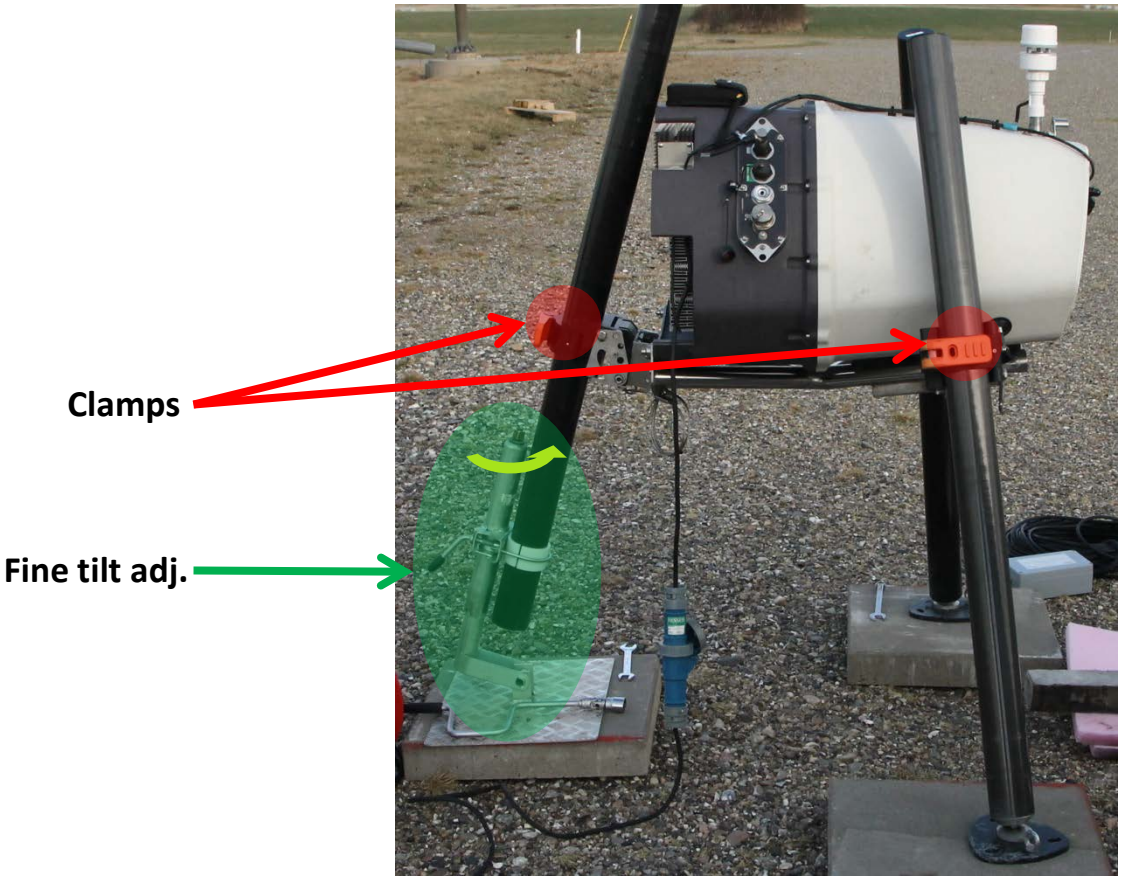

Figure 25. Fine tilt adjustment system used for the ZDM lidar

Annex E. Høvsøre wind rose

The wind climate in DTU's test section, Høvsøre, on the West coast of Jutland is the figure below.

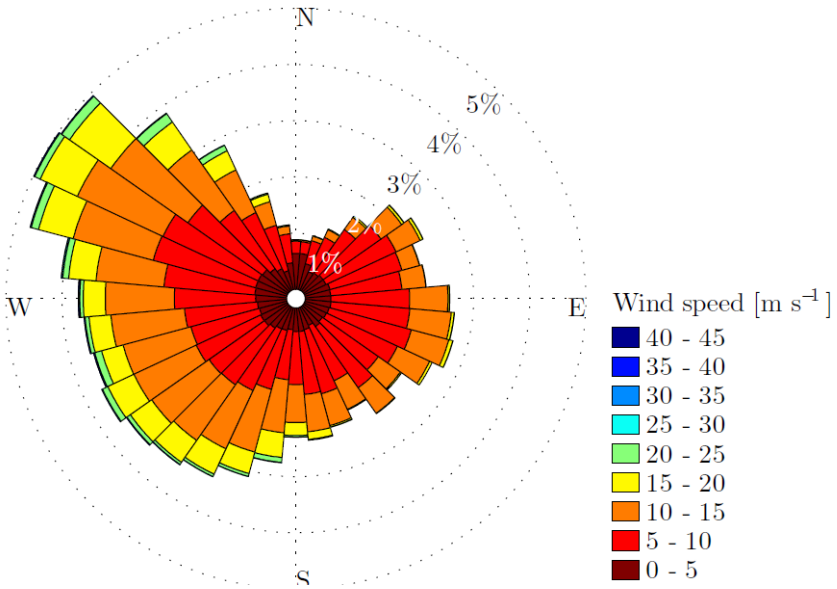

Figure 26. Wind rose at 100m in Høvsøre, between 2005-2013

(Reproduced with permission from A. Penã, extracted from [9])

Annex F. SQL query to average RAW data

```sql
create table zephir351_10min_tmp_2degPhase
select min(u.`Reference`) as Reference_min,
u.`Name` as Name,
u.`Phase_bin` as Phase_bin,
u.`Range` as `Range`,
count(u.`Reference`)/600 as availability_LOS,
sum(u.`Raining`) as Raining_sum,
avg(u.`Phase`) as Phase_avg,
std(u.`Phase`) as Phase_avg_stdv,
min(u.`Phase`) as Phase_avg_min,
max(u.`Phase`) as Phase_avg_max,
avg(u.`LOS_velocity`) as LOS_velocity_avg,
std(u.`LOS_velocity`) as LOS_velocity_stdv,
min(u.`LOS_velocity`) as LOS_velocity_min,
max(u.`LOS_velocity`) as LOS_velocity_max,
avg(u.`tilt_deg`) as Tilt_avg,
std(u.`tilt_deg`) as Tilt_stdv,
min(u.`tilt_deg`) as Tilt_min,
max(u.`tilt_deg`) as Tilt_max,
avg(u.`roll_deg`) as Roll,
std(u.`roll_deg`) as Roll_stdv,
min(u.`roll_deg`) as Roll_min,
max(u.`roll_deg`) as Roll_max,
avg(u.`Fore_Aft_Velocity`) as Fore_Aft_Velocity_avg,
avg(u.`Spectral_spread`) as Spectral_spread_avg

from hovsore_naclidar.unitte_zephir351_raw u
where u.Name between '201502061300' and '201503240000'
and u.`Phase` between 179.0 and 181.0
group by u.`Name`, u.`Range`
```

Annex G. Table of calibration results

The results presented in the tables below are obtained by applying the same calibration procedure but with two different reference wind speed instruments, i.e. cup and sonic anemometers:

- Cup anemometer used for reference wind speed in:
  - Table 4: filtered 10-minute RWS data ("raw") ;
  - Table 5: binned RWS data ;
- Sonic anemometer used for reference wind speed in:
  - Table 6: filtered 10-minute RWS data ("raw") ;
  - Table 7: binned RWS data.

Table 7. Raw calibration results: ZDM unit 351 ; HWS measured by cup anemometer

	Azimuth sector ° / LOS	Range selected [m]	LOS dir [°]	Valid data points	Raw calibration					TI range	T abs 2m range
					"Free" regression			Forced regression			
					gain	offset	R2	gain	R2		
ZDM	179-181	253	287,44	2140	1,0097	-0,0644	0,9979	1,0022	0,9978	10-17%	3-8°C
	178-182	253	287,45	2140	1,0097	-0,0633	0,9979	1,0023	0,9978	10-17%	3-8°C
	177-183	253	287,48	2140	1,0098	-0,0644	0,9980	1,0023	0,9979	10-17%	3-8°C
	176-184	253	287,46	2140	1,0100	-0,0622	0,9979	1,0027	0,9979	10-17%	3-8°C
	175-185	253	287,49	2140	1,0104	-0,0641	0,9980	1,0029	0,9979	10-17%	3-8°C

Table 8. Binned calibration results: ZDM unit 351 ; HWS measured by cup anemometer

	Azimuth sector ° / LOS	Range selected [m]	LOS dir [°]	Valid data points	Binned calibration					range of valid bins [m/s]		TI range	T abs 2m range
					"Free" regression			Forced regression					
					gain	offset	R2	gain	R2	min	max		
ZDM	179-181	253	287,44	2140	1,0167	-0,1212	0,9999	1,0050	0,9998	3	15	10-17%	3-8°C
	178-182	253	287,45	2140	1,0168	-0,1212	0,9999	1,0051	0,9998	3	15	10-17%	3-8°C
	177-183	253	287,48	2140	1,0163	-0,1168	0,9999	1,0050	0,9998	3	15	10-17%	3-8°C
	176-184	253	287,46	2140	1,0166	-0,1160	0,9999	1,0054	0,9998	3	15	10-17%	3-8°C
	175-185	253	287,49	2140	1,0168	-0,1158	0,9999	1,0056	0,9998	3	15	10-17%	3-8°C

Table 9. Raw calibration results: ZDM unit 351 ; HWS measured by sonic anemometer

	Azimuth sector ° / LOS	Range selected [m]	LOS dir [°]	Valid data points	Raw calibration					TI range	T abs 2m range
					"Free" regression			Forced regression			
					gain	offset	R2	gain	R2		
ZDM	179-181	253	288,35	2139	1,0055	-0,0663	0,9976	0,9977	0,9976	10-17%	3-8°C
	178-182	253	288,37	2139	1,0054	-0,0650	0,9977	0,9978	0,9976	10-17%	3-8°C
	177-183	253	288,37	1989	1,0057	-0,0652	0,9977	0,9981	0,9977	10-17%	3-8°C
	176-184	253	288,37	2112	1,0059	-0,0645	0,9977	0,9984	0,9976	10-17%	3-8°C
	175-185	253	288,40	1862	1,0062	-0,0636	0,9978	0,9989	0,9977	10-17%	3-8°C

Table 10. Binned calibration results: ZDM unit 351 ; HWS measured by sonic anemometer

	Azimuth sector ° / LOS	Range selected [m]	LOS dir [°]	Valid data points	Binned calibration					range of valid bins		TI range	T abs 2m range
					"Free" regression			Forced regression					
					gain	offset	R2	gain	R2	min	max		
ZDM	179-181	253	288,35	2139	1,0156	-0,1424	0,9999	1,0019	0,9997	3	15	10-17%	3-8°C
	178-182	253	288,37	2139	1,0155	-0,1407	0,9999	1,0019	0,9997	3	15	10-17%	3-8°C
	177-183	253	288,37	1989	1,0152	-0,1375	0,9999	1,0020	0,9997	3	15	10-17%	3-8°C
	176-184	253	288,37	2112	1,0154	-0,1365	0,9999	1,0023	0,9997	3	15	10-17%	3-8°C
	175-185	253	288,40	1862	1,0154	-0,1329	0,9999	1,0026	0,9997	3	15	10-17%	3-8°C

References

[1] Wagner R.: "Accounting for the speed shear in wind turbine power performance measurement", [2010], Risø-PhD-58(EN), ISSN: 1095-4244 (*http://dx.doi.org/10.1002/we.509*), vol: 14, issue: 8, pages: 993-1004, 2011.

[2] Wagner R., Pedersen T.F., Courtney M., Antoniou I., Davoust S., Rivera R.L.: "Power curve measurement with a nacelle mounted lidar", [2014], Wind Energy, Vol: 17, issue: 9, pages 1441–1453 (*http://dx.doi.org/10.1002/we.1643*).

[3] Borraccino A., Courtney M., Wagner R.: "Generic methodology for calibrating profiling nacelle lidars", [2015], DTU Wind Energy E-0086.

[4] Courtney M.: "Calibrating nacelle lidars", [2013], DTU Wind Energy E-0020(EN).

[5] JCGM 200:2012: "International Vocabulary of Metrology – Basic and General Concepts and Associated Terms" (VIM 3rd edition), (http://www.bipm.org/en/publications/guides/vim.html)

[6] JCGM 100:2008: "Evaluation of measurement data – Guide to the expression of uncertainty in measurement" (GUM), (http://www.bipm.org/en/publications/guides/)

[7] Westermann D., Rehfeldt K.: "Summary of cup anemometer classification" (for Thies First Class Advanced), Deutsche WindGuard GmbH (http://www.thiesclima.com/Anemometer%204.3351.%20classification%2012%202008%20.pdf)

[8] IEC 61400-12-1: Draft CDV, 30 April 2014, "Power performance measurements of electricity producing wind turbines"

[9] A. Penã et. Al: "Ten years of boundary-layer and wind-power meteorology at Høvsøre, Denmark" (*http://dx.doi.org/10.1007/*s10546-015-0079-8)